Kristina Shizuka Yamase Skarvang

Meteor Radar Observations of the Atmospheric tides

Master's thesis in Physics
Supervisor: Prof. Patrick J. Espy
September 2020

Norwegian University of Science and Technology
Faculty of Natural Sciences and Technology
Department of Physics

NTNU | Norwegian University of Science and Technology

Acknowledgements

I would like to give a special thanks to my supervisor Prof. Patrick Joseph Espy, for all his advice and encouragements, in addition to giving me such an exciting project. I also would like to thank Prof. Robert Hibbins for providing me with a lot of helpful advice, ideas, and information in analysing the data. Thanks to Wim vam Caspel for helpful input, advice, and feedback. Thanks also to Dr Stefan Bender for giving me advice, especially on how to present data. I thank my parents and also my extended family for encouraging and supporting during studies in many aspects, Kjetil Arne Vaskinn for proofreading, and also Sveinung Heide Vaskinn who supported me through hard times and helping me a lot with data handling.

Abstract

This thesis investigates the possibility of interhemispheric coupling of atmospheric waves during Sudden stratospheric warming (SSW) event. Meteor Radar located at Rothera (68°S, 68°W) on the Antarctic Peninsula has been used to measure the wind from 82km to 98km altitude, and the data covers data from February 2005 to August 2019 with a spectra resolution of 1 hour and an altitude resolution of 2km. Curve fitting was performed to find the individual components of atmospheric tides, and the climatology of 2-days planetary waves, diurnal waves, semidiurnal waves, terdiurnal waves, and the mean background wind were analysed. Then, superposed epoch analysis (SPE) was performed around the SSW onset to investigate whether there is a reaction. Data from this project showed a negative response in the semidiurnal tide after the SSW onset and an enhancement in the 2-days planetary waves after the SSW onset. The same analytical method was used to analyse the response in the atmosphere at Rothera to magnetic storms. There was some hint of post-storm enhancement in the diurnal and semidiurnal wind; however, the maximum enhancement was around 2σ.

Sammendrag

Denne oppgaven undersøker muligheten for interhemisfærisk kobling av atmosfæriske bølger under ”Sudden stratospheric warming” (SSW) hendelser. Meteor-radar lokalisert ved Rothera (68°S, 68°W) på Antarktishalvøya har blitt brukt til å måle vinden fra 82 km til 98 km høyde, og dataene dekker datoene fra og med februar 2005 til og med august 2019 med en tidsoppløsning på 1 time og en høydeoppløsning på 2 km. Kurvetilpasning ble utført for å finne de enkelte komponentene i atmosfæriske luftbølger. Videre ble klimatologien til todagers planetære bølger, døgnbølger, halvdøgnbølger, åttetimersbølger, og gjennomsnittlig bakgrunnsvind analysert. Deretter ble ”Superposed epoch analysis” (SPE) utført rundt starten av SSW-hendelsene for å undersøke om det finnes noen respons ved Rothera. Data fra dette prosjektet viste en negativ respons i halvdøgnbølger og en positiv respons i todagers planetære bølger etter SSW. Den samme analysemetoden ble brukt til å analysere responsen i atmosfæren, på magnetiske stormer, ved Rothera. Det var noe antydning til positiv respons etter stormene i døgn- og halvdøgnvinden; største avvik var imidlertid kun rundt 2σ.

Table of Contents

List of Tables

List of Figures

Abbreviations

Dst	=	Disturbance storm-time
GW	=	Gravitaional waves
IGY	=	International Geophysical Year
MLT	=	Mesosphere and lower thermosphere
PW	=	Planetary waves
QTDW	=	Quasi-two-day wave
SDT	=	Semidiurnal Tide
SkiYMET	=	All-Sky Interferometric Meteor
SPE	=	Superposed Epoch Analysis
SSW	=	Sudden Stratospheric Warming
WACCM	=	Whole Atmospheric Community Climate Model

Chapter 1

Introduction

Our lives are greatly affected by the continuously changing Earth's atmosphere. Therefore, there has been much interest and research in understanding and predicting the motion of the Earth's atmosphere. While there have been systematic studies on the troposphere, where violent and vigorous motions occur, it is not the case that the troposphere is the most active region in the atmosphere. Unlike the troposphere, where the temperature decreases with height, the stratosphere is a region where the temperature increases with height. Therefore, the stratosphere is stable against the vertical motion of the air due to adiabatic changes. In other words, active heat convection does not occur in the stratosphere and it is stratified in temperature. Hence the name "stratosphere" is given to this region.

However, the stratosphere is not a region where there is no atmospheric motion, but rather various atmospheric phenomena occur. Sudden Stratospheric Warming (SSW) that occurs in the stratosphere at high latitudes in the Northern Hemisphere is one of the phenomena. SSW are a sudden increase in the stratospheric temperature and is thought to be caused by the momentum carried by waves from the troposphere.

The region above the stratosphere, and especially between 80 and 100km, is the least studied part of the atmosphere and is often called "ignoro-sphere" [10]. Studying this region will give us more insight into the interaction between the layers in the atmosphere, which is essential to improve climate and weather models.

In this study, a Meteor Radar in Antarctica, Rothera is used in order to obtain the amplitudes of the atmospheric wave components. Various studies have studied the reaction to SSW of the atmospheric wave components in the Northern hemisphere. In recent sutdies, Hibbins et al. (2019) [11] have studied the responce of the semidiurnal tide (SDT) to SSW and showed an enhancement around 10-17 days after the SSW onset. Stray et al. (2014) [12] have observed the Planetary wave (PW) activity in the Mesosphere-lower Thermosphere (MLT) during SSW and significant enhancement after onset was found. In this project, the aim is to study the reaction of the atmosphere in the Southern Hemisphere. We attempt to understand the dynamics in the MLT and mechanism of interhemispheric coupling by studying the response of the atmospheric wave components in the Southern

Hemisphere for an event that occurs mostly in the Northern Hemisphere.

Chapter 2

Theory

2.1 The Atmosphere

2.1.1 Vertical Structure of the Atmosphere

One of the methods of classifying the earth's atmosphere is the method based on atmospheric temperature, which has been carried out based on observational data since the beginning of the 20th century [13]. According to this method, the earth's atmosphere is divided into four regions; troposphere, stratosphere, mesosphere and thermosphere, as shown in Figure 2.1.

- **Troposphere**
  The troposphere is the region of the atmosphere at an altitude of about 15 km from the ground. The atmospheric temperature is about 300K-220 K. There is no heat source in this region other than the ground surface heated by the Sun. Therefore, the atmospheric temperature decreases almost unidirectionally (about 6.5 K/km) as the altitude increases. Heat in this region is carried by convection.

- **Stratosphere**
  The stratosphere is the region from the tropopause to an altitude about 50 km. The atmospheric temperature is about 220K-270K. In contrast to the troposphere, the temperature increases with altitude. This is mainly due to the heating effect of ozone absorption by UV light. The temperature structure of the stratosphere is determined by the balance between this heating effect and the cooling effect of carbon dioxide, water vapour and infrared radiation of ozone.

- **Mesosphere**
  The mesosphere is the region from the stratopause to an altitude of about 90 km. The atmospheric temperature is about 270 K to 180 K. The temperature decreases in this region and reaches its minimum at the mesopause. The temperature structure in this region is balanced by the absorption heating of UV radiation from oxygen molecules

and the cooling of carbon dioxide infrared (15μm) and ozone infrared (9.6μm) radiation. In addition to these, atmospheric waves such as internal gravitational waves (GW) and planetary waves (PW) propagated from the lower atmosphere, turbulence, and heat conduction drive this region far from radiative equilibrium and continue into the thermosphere.

- **Thermosphere**
  The thermosphere is the region from the mesosphere interface to an altitude of 600 km. The temperature rises to about 600 km altitude and is almost constant above that altitude (the exosphere). In the thermosphere, the atmosphere is heated by the absorption of extreme ultraviolet (EUV) radiation and X-rays. The temperature in the thermosphere varies with solar activity. Significantly above 200 km altitude, this variation is in the order of tens of per cent.

The atmosphere is a mixture of gases. Table 2.1 shows the composition of the air near the Earth surface.

Species	**Dry Air [Vol%]**	**Wet Air [Vol%]**
N_2	78.1	77.0
O_2	21.0	20.7
Ar	0.9	0.9
CO_2	0.04	0.03
Ne, He, Kr, H_2, O_3, SO_3	<0.01	<0.01
H_2O	-	1.3

Table 2.1: Composition of the air near surface [1]

The gas composition in the atmosphere for major species ($<0.04\%$) remains the same up to about 100 km altitude due to the turbulence effect and is mainly composed of nitrogen and oxygen molecules. Beyond 100 km altitude, the oxygen molecules are dissociated into oxygen atoms by photodissociation, and the light particles move upward. At altitudes up to about 150 km, molecular gas is the main species of the atmosphere, but above that altitude, oxygen atoms are the main species. In the exosphere, the main components are helium and hydrogen. [13]

2.1.2 Circulation in the Atmosphere

Although the atmosphere is devided into layers as explained above, it does not mean that there are horizontal lines between the parts. The energy of the atmosphere can circulate in the atmosphere. This section explains about the circulation in the atmosphere and its effect based on the webpage of Tokyo University, Prof. Sato's group [14] and Nora Stray's doctral thesis [15]. The atmosphere at an altitude of about 10 to 100 km above the troposphere (stratosphere, mesosphere, and lower thermosphere) is called the middle atmosphere. Figure 2.2 shows the zonal mean temperature in the latitudinal height cross-section of the Earth's atmosphere at the solstice, expressed in colours. In January, the temperature distribution in the northern and southern hemispheres is almost opposite, with summer in the

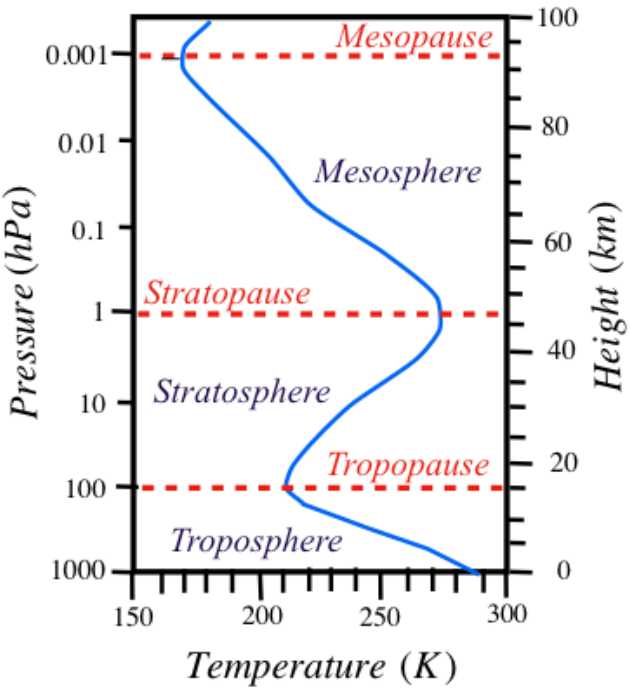

Figure 2.1: Vertical structure of atmospheric temperature (K) in the lowest 100km of the atmosphere. [4]

northern hemisphere and winter in the southern hemisphere.
The stratopause (the maximum temperature at high altitude) can be seen at around 50 km. This is because the ozone layer absorbs the solar ultraviolet radiation and warms the atmosphere at that height. This is known as ozone heating. Because the ozone layer is unique to Earth, created by living organisms, the stratospheric interface is not found on the atmospheres of other planet. The maximum temperatures at the stratopause are found in the summer polar regions. In July, solar radiation at culmination is strongest at 20°N, but the sun does set in that latitude. Because of the 24-hour heating in the polar regions in summer, the daily solar radiation received by the poles is greater than at any other latitude. This is the reason for the summer temperature maximizing at the polar stratospheric interface. Then there are two interesting features. One is that there is a stratopause at the winter poles (the southern polar region in Figure 2.2). This region would be at polar night during the winter. Another feature is that the temperature is low at the mesopause at the summer poles (the northern polar region in Figure 2.2). The temperature here is the lowest in the Earth's middle atmosphere. Also, because it is cold, even a little water vapour (created by the oxidation of methane) freezes and forms clouds. This is called a noctilucent cloud because it glows in the middle of the night. In summer, the polar mesopause is also midnight, but in winter, the polar mesopause is warmer. The cause of these temperature

characteristics is the general atmospheric circulation. The yellow lines in Figure 2.2 shows the general circulation in the middle atmosphere. In the stratosphere, there are two circulations from the low latitudes to the poles (called the Brewer-Dobson circulation), and in the middle atmosphere, there is a large circulation from the summer pole to the winter pole. At the winter pole, both the stratosphere and the mesosphere have downward currents, and at the summer pole, the stratosphere has downward currents, and the mesosphere has upward currents. These currents moving up and down can significantly change the temperature. The higher the altitude, the lower the atmospheric pressure becomes. At ground level, the pressure is about 1000 hPa, but it decreases to about 100 hPa at 15 km, 10hPa at 30 km, 1hPa at 50km, and about 0.01 hPa at 80 km height. Therefore, when the air at the bottom is lifted by upward motion, the temperature drops due to adiabatic expansion, and when the air at the top is pushed down by downward motion, the temperature rises due to adiabatic compression. This is the mechanism for maintaining low temperatures in the polar mesosphere in summer and high temperatures at the polar stratopause in winter. The reason that this circulation exists is because atmospheric waves occur mainly in the troposphere and propagate into the stratosphere and mesosphere, giving momentum to the atmosphere. This is also known as wave drag, or wave resistance because it acts like friction. However, it can also have negative friction, so it is better to call it a wave-forcing. This wave forcing creates the meridional cycle because the Earth is nearly spherical and is rotating. Due to the circulation in the atmosphere, studying MLT region of the atmosphere is connected to understanding the whole atmosphere on the earth.

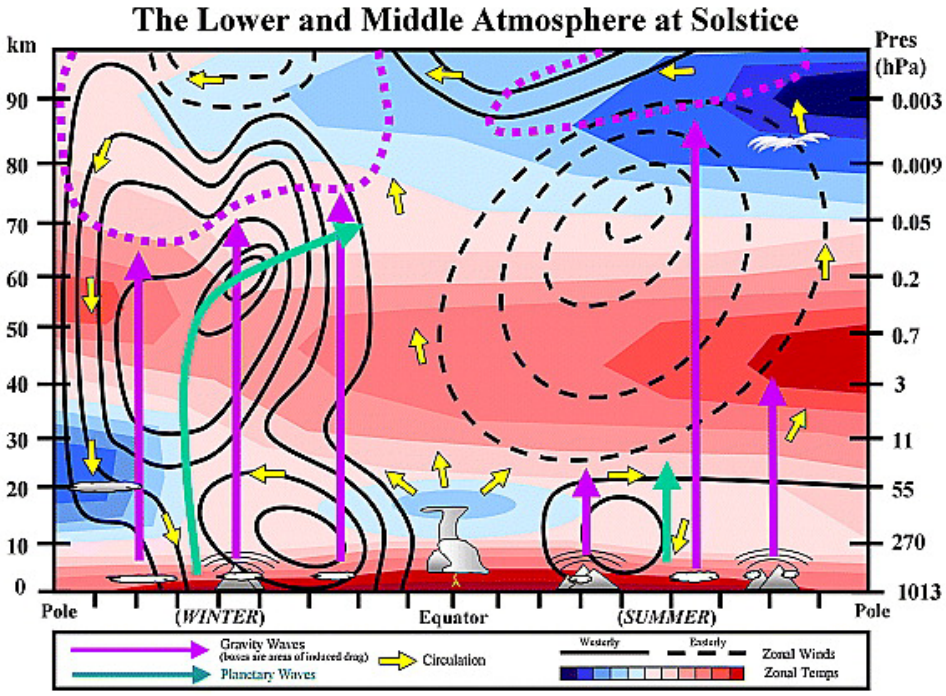

Figure 2.2: Latitudinal altitude cross section of the mean east-west temperature [5]

2.2 Atmospheric Waves

Atmospheric motions are superimposed by the average wind system, as determined by the temperature structure and Coriolis forces, by various atmospheric waves with sources of excitation at the surface, troposphere and stratosphere. These atmospheric waves propagate upward, agitating objects and transporting momentum and energy to the upper atmosphere. As the altitude increases, the atmospheric density decreases. Since the energy of the atmospheric wave motion ($E = mgh$) is conserved, the amplitude of the wave increases with altitude. Eventually, the waves break up and dissipate momentum and energy. Atmospheric waves have various periods and can be roughly divided into three main types, atmospheric gravity waves, atmospheric tidal waves, and planetary waves, depending on their characteristics. This project focuses mainly on atmospheric tidal waves and planetary waves.

The atmospheric tides are periodic motions of the earth's atmosphere caused by the radiation of the sun to the atmosphere. Ozone (Stratosphere), water vapours (Troposphere), and oxygen molecules (Thermosphere) absorbs the radiation from the sun and warms up the atmosphere. It is also called tidal wind, because it is observed as a significant change in atmospheric pressure and wind, especially in the stratosphere and mesosphere and thermosphere of the middle atmosphere. Tidal winds are on a continental scale and are characterized by a daily cycle of rising and falling pressure.

When one spot of the atmosphere is heated by the sun, that point expands, and that creates a pressure gradient between the adjacent air and forces the wind from the hottest point to colder areas on the planet. As the heated spot shifts across the earth following the sun, it creates a wave that propagates Eastward together with the sun.

The tides in the atmosphere are not only 24h wave, but we see 12h and 8h waves as well. In some latitudes, the 24h wave is the strongest, and in other latitudes, the 12h waves are the strongest. Mathematically, the tide components can be written as a Fourier decomposition with an assumption that the heating at any point on the earth is not sinusoidal, but 0 during the night and half-cycle during the day. [16].

$$J(t) = \sum_{n=0}^{N} A_n(\theta, z, \lambda) \sin\left(n\Omega t - \phi_n(\theta, z)\right) \tag{2.1}$$

Here, $\Omega = \frac{2\pi}{24}$, t is in hours, A_n and ϕ_n represents the amplitude and the phase of the tidal heating, z is height, θ is latitude, and λ is longtitude. Different values of n seperate the different atmospheric wave components, which are called diurnal ($n = 1$), semidiurnal ($n = 2$), and teridiurnal ($n = 3$) which are used in this project.

In reality, the air is fluid as a thin coating on a hard-sphere, so it has a three-dimensional aspect to it. Thus the air moving northward from the heating bulge will eventually meet the air that has moved southward from the heating bulge via the other side of the earth. This interaction generated all sorts of harmonics with different spatial and temporal wavelengths which also circulate.

As explained earlier, not only ozone in the stratosphere but the water vapours in the troposphere and the oxygen molecules in the thermosphere can heat and launch a wave. These waves interact and create a vertical interference pattern, and the higher harmonics interfering with each other also create a vertical structure. As a result, the diurnal wave cancels at

latitudes far from the equator, and the semidiurnal wave maximizes at higher latitude.
The atmospheric tidal waves can have a wavenumber 1 (non-migrating) and wavenumber 2 (migrating) as well as higher wavenumbers. The migrating wave moves in longitude at the same speed as the sun, so at any fixed longitude, two peaks and two valleys come over in 24 hours, which is 12h wave. The non-migrating semidiurnal tide moves around the earth twice as fast as the sun is moving, which will also produce a 12h wave. These two waves will interfere with each other negative and positive at different longitudes, which are not able to separate in a single station measurement like this project.
Planetary waves (PW) are induced by vital forces such as Coriolis forces, which are caused by instability in a moving air mass due to temperature gradients. The waves are global in scale. These waves are very pronounced in the stratosphere. Although the amplitude intensity is usually smaller than that of atmospheric tidal waves, it plays an essential role in MLTs, considering the inter-wave interaction. PW in a period of 2 days is called quasi-two-day wave (QTDW)

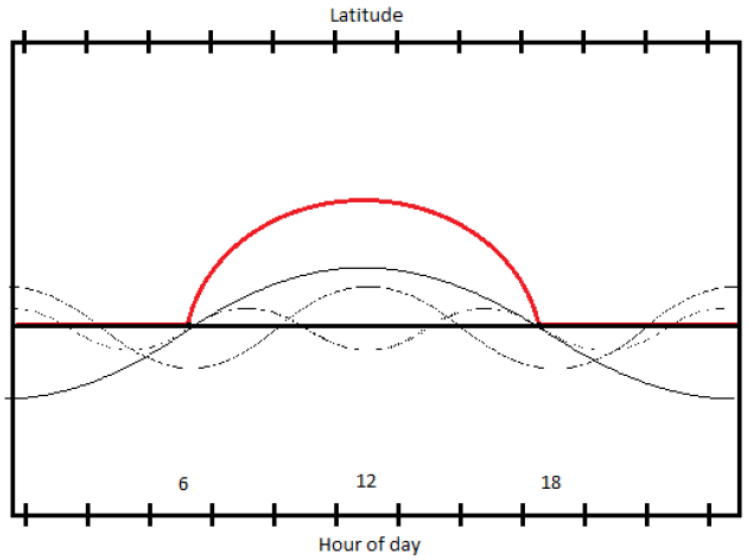

Figure 2.3: Illustration of the different wave components of the wind (black) that are produced by the heating (red) [6]

2.3 Sudden Stratospheric Warming

A Stratospheric Sudden Warming (SSW) is a phenomenon in which the temperature increases suddenly in the stratosphere. This is a dramatic event since stratosphere is the region where daily temperature changes are slow. In February 1952, Scherharg of the Free University of Berlin, who was conducting radiosonde observations of the stratosphere in Germany, discovered that the stratospheric temperature increases by more than 40 degrees

Celsius in a few days. What is interesting is that the rise in temperature starts earlier in the upper layers, and it gradually weakens as it moves downward.
Since it had been believed until then that stratospheric motions would not occur in the stratosphere, it is surprising that such violent temperature changes were observed in the stratosphere as well. At first, it was suspected that this phenomenon was different from ordinary atmospheric phenomena and was caused by changes in solar activity, such as magnetic storms in the ionosphere and northern lights. However, as the world's stratospheric observation networks were established, it became clear that SSW was not merely a local phenomenon, but a cataclysmic change in the stratospheric circulation that covered the entire northern hemisphere.
The outbreak of SSW is said to be induced by the planetary wave deriving at the troposphere and propagating upward. Planetary waves are one of the westerly wind waves, which the amplitude can suddenly be enhanced by the heating of the atmosphere and the undulations of the terrain. One of the characteristics of planetary waves is that when the zonal mean wind is easterly, it is difficult to propagate upward, but when it is westerly, it can propagate upward with almost the same energy density. As mentioned earlier, the energy conserves, but the density of air becomes gradually lower by propagating upwards, so the amplitude of the wind becomes larger, and the non-linearity of the wave becomes stronger. Due to this non-linear effect, a mean wind westward acceleration at the end of the wave occurs. That means, the eastward wind decreases, and the southward Coriolis force working to the eastward wind decreases. Therefore, there will occur a northward movement, and in order to adjust the ballance, in the converging vertical flow will occur at the lower latitude, and a diverging vertical flow will occur at the highter altitude. Becuase of the downward stream of the downside of the diverging flow in the higher latitude, adiabatic compression occurs, and the temperature rises in the stratosphere. Because there are more variations in the landform and conversion between water and land in the Northern hemisphere than the Southern hemisphere, SSW is more likely to occur in the Northern hemisphere. When the eastward wind gets westward acceleration, it will gradually turn into eastward wind. Above the altitude where the wind turns from eastward to westward, the planetary wave attenuates, so the altitude where the temperature rises sinks according to time. When the altitude of the phenomenon moves down, the amplitude of the planetary wave becomes smaller due to the density of air. Therefore, the temperature rising rate becomes smaller in lower altitude. The process from the propagation of planetary waves to the onset of SSW is qualitatively explained by Matsuno and Shimazaki (1981).

2.4 Magnetic Storm

Electron energies from about 2 to 20keV cause the northern light. The electrons from the solar wind, plasma flowing from the sun, have been captured on the outer surface of the magnetosphere. This solar wind plasma carries the magnetic field of the sun inside of it, and when it hits the Earth's field, the two fields can merge, transferring the plasma onto the Earth's field lines. It becomes energized to 2-20keV in outer magnetosphere processes. When it enters the Earth's atmosphere, it penetrates down at far as 90km altitude, but the average penetration is typically 105km altitude. When this occurs, currents flow at these

altitudes that can perturb the surface magnetic field under the northern lights.
When some more massive storms, a high-density solar wind, hit the Earth, some plasma can also be transferred to the radiation belts in the inner magnetosphere. These are closed field lines and processes in this area can raise the electron energies to 30keV and up to MeV order. These can enter the atmosphere at slightly lower latitudes than the auroral electrons, and because of their higher energy, the electron can penetrate deeper into the atmosphere, down to around 70km altitude. Because the elevated plasma density on these field lines can rotate with the Earth, one sees a ring current at the equator.
The Disturbance storm-time (Dst) index was developed to give an indication to ring current strength. The Dst index has been found in the definition of the storm variation, $D = Dst + DS$ where DS can be thought of as being due to auroral electrojet activity. The original International Geophysical Year (IGY) Dst index was obtained by using the network of eight geomagnetic observatories near the equator listed in Table 2.2. The observatories locations were chosen based on measurement quality, sufficient distance from the influence of both auroral and equatorial electrojets, and a uniform distribution in longitude. Data is available back to 1957, the temporal resolution is 1h, and the index is expressed in nT. Measurements are mainly of the ring current intensity, and the tail current and the magnetopause Chapman-Ferraro current are removed at each observatory as they influence the data since they are all in the equatorial plane. The Dst index is prepared by calculating the variation in horizontal (H) component of the terrestrial magnetic field, which is done for each observatory individually before the hourly Dst for each observatory is averaged and normalized with respect to the dipole equator. The quiet solar time is found by averaging the five most quiet days of the month. Negative Dst indicates an enhanced ring current, which induces a magnetic field directly opposite to the Earth's magnetic field. The induced field weakens the geomagnetic field and reduces the H measured on the surface at equatorial and mid-latitudes. The strength of the horizontal component on the surface is inversely proportional to the energy content of the ring current, the magnitude of the decrease in H, therefore, represents the severity of disturbance. Favourable variations in Dst are mostly caused by the compression of the magnetosphere from increases in the solar wind pressure. [2] [3] [17]

Station	North Latitude	East Longitude	Comment
Hermanus	-33.3	80.3	IGY and after
Alibag	9.5	143.7	IGY only
Kakioka	26.0	206.0	IGY and after
Apia	-16.0	206.0	IGY only
Honolulu	21.0	266.4	IGY and after
San Juan	29.9	3.2	IGY and after
Pilar	-20.2	4.6	IGY only
M'Bour	21.2	55.1	IGY only

Table 2.2: Observatories Used for Computation of Equatorial Dst [2] [3]

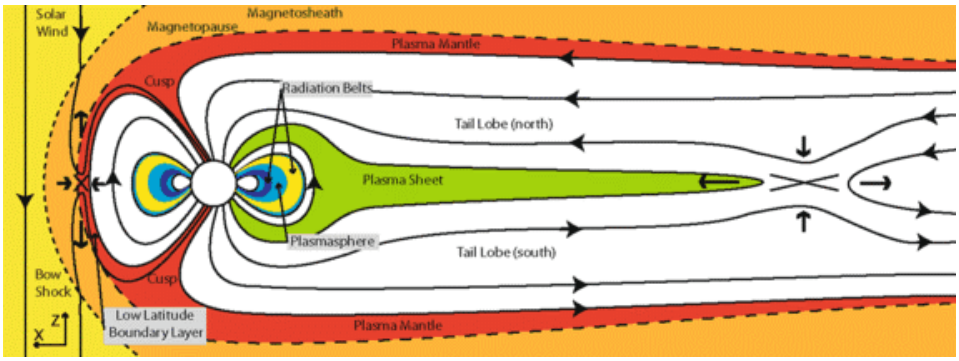

Figure 2.4: Illustration of Earth's magnetosphere [7]

Chapter 3

Instruments

3.1 Meteor Radar

The purpose of this project is to observe the atmospheric waves in the least studied region, 80 to 100km altitude. In order to receive information about this region, weather balloons are not high enough, and satellites have difficulty in giving continuous measurement. Therefore, data from a Meteor Radar was used in this project, since it is capable of continuous measurement in this altitude. The data used in this project comes from a Meteor Radar located at Rothera ($68°$S, $68°$W) on the Antarctic Peninsula. It is a SkiYMET meteor radar deployed in February 2005. The radar measures the winds of the MLT regions of the atmosphere. The Meteor Radar works in the same way as the SKiYMET radar located at Dragvoll, Trondheim, which the performance is summarized in Rosmarie J. de Wit's Doctoral thesis [10] and a general description of meteor radar can be found in the article by W. K. Hocking et al. (2001) [18] [19]. The Meteor Radar has eight transmitter antennas and five receiver antennas which sends out pulses of frequency 1kHz. The eight transmitting antennas are distrubuted in a circular form which focuses the transmittion to the zenith angle between $10°$ and $90°$. Due to the setup, there are interference for azimuth angles every $45°$. The five receiving antennas are set up as a cross with one in the middle. Every day, 30 to 100 tonnes of meteors enter the atmosphere. When a meteor enters the atmosphere, the trails last for about four seconds as they burn up in the atmosphere at about 90km altitude, and the wind will drift the ionized trail. The echos of that trail will come back to the receivers. Two of the receivers gives the North and South orientation of that trail, and the other two gives East and West orientation to localize the spot in the sky. Each receiver records the received data for 6 seconds and saves the segment of data if it catches something. In this way, you get not only the amplitude but the direction. The radar software processes the information from each receiver and produces hourly wind data file including the information of the line of sight velocity. A detailed description in how to convert the received signal to meteor position and radial velocity using hardware and software can also be found in Hocking et al. (2001) [18]
Figure 3.1 shows the typical meteor trail pattern observed over a 24 hour period in terms of

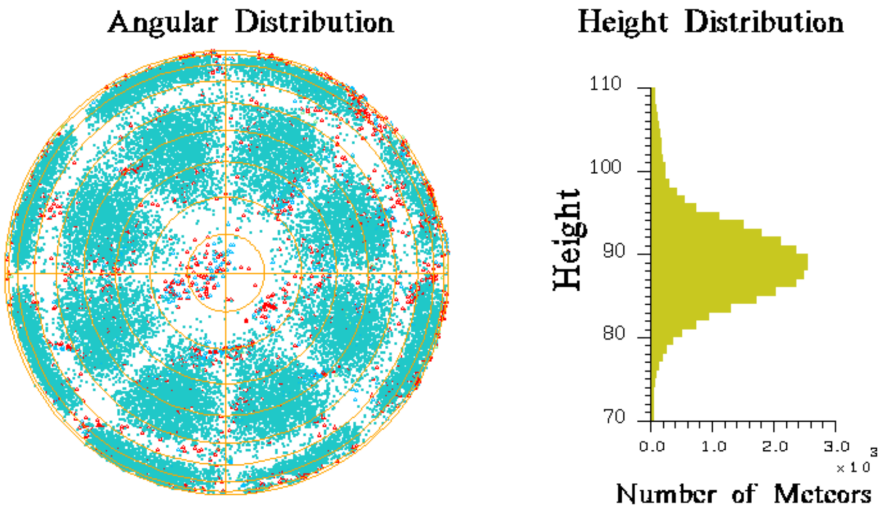

Figure 3.1: Typical angular distribution (left, $10°$-$90°$ zenith angle) and height (right, 70km-110km altitude) distribution for detected meteors. [8]

azimuth and zenith angle (left) and the height distribution of detected meteors in the same time-frame (right). It shows that the most unambiguous meteors are observed between $15°$ and $50°$, and that detected meteors are peaking at around 90km.

Chapter 4

Analysis

4.1 Climatology

The data gathering for this project was done from February 2005 to August 2019 in the Antarctica, Rothera station, with an hourly mean wind data as a function of altitude. MATLAB R2019b was used to analyse the data and make the plots. In order to separate the background mean wind, the two-days planetary wave, the diurnal tide, the semidiurnal tide, and the terdiurnal tide, a fitting routine was performed. One takes four days of data to which a mean wind, the 8, 12, and 24 hours tidal components, and the 48-hour QTDW are fitted by assuming that there is no vertical component of the wind. This was done by using a least-square routine in MATLAB which is expressed by the following equation with U (Zonal) and V (Meridional) wind components. [6]

$$V_{LOS} = U \cdot \cos\theta \cos\phi + V \cdot \sin\theta \sin\phi \tag{4.1}$$

V_{LOS} are the line of sight velocity, θ are the zenith angle, ϕ are the azimuth angles of the meteors detected. For the tidal components, the standard phase information was converted to the hour of the first maximum in the tide. A negative amplitude has been shifted as a phase shift of an additional $90°$. Thus, the phase can be converted to the hour of the first maximum in the sine wave.
In addition to sorting the amplitudes to positive, all the wind data were quality checked whether there is enough data spread relatively evenly over the four day periods to assure the data quality. [12] Following Stray et al. (2014), the quality check was performed as written below.

- Exclude the winds over 150m/s
- Segments must cover at least half of the hour and spanning at least in 16 different hours
- 4 day segments that have data gap >3h that occurs at the same hour in each day of that segment are excluded

- 4 day segments with data gaps >12h that covers the same hours in both halves of the segment are excluded

Upon completion of curve-fitting, the 4-day window is shifted by one day, and phase sorting, quality check, and wave fitting are repeated. This gives a mean amplitude and phase on a daily basis, smoothed over four days.
In order to obtain the climatology, starting with 1st January as day 1 in the year, the average value of each day for 365 days were calculated. Then the average points for 365 days was repeated 3 times, smoothed using 'smoothing spline', and the middle smoothed average was taken as a climatology. This secures the continuous smoothing even at the end (beginning and end of the year).

4.2 Superposed Epoch Analysis

In order to investigate the effect to the Southern Hemisphere of SSW that is usually a northern event, Superposed Epoch Analysis (SPE) was performed. SPE is also called composite analysis or Chree analysis, and is used in numerous fields as geostatistics, fluid dynamics, and plasma physics. It is a very useful procedure in obtaining information concerning periodicities or for understanding the relationship between two phenomena. [20] [21]
Once the climatology of the data for this project is derived, the anomaly of the data is given by subtracting the repeated climatology from the original data (15 years in this project) as shown an example in Figure 4.1.
After the anomaly is derived over the whole data, we pick up the SSW onset dates and collect a time frame from 20 days before the onset to 20 days after the onset as in Figure 4.2. All the SSW onset 41 days frame will be averaged to see whether there are effects to the tidal components in Rothera.

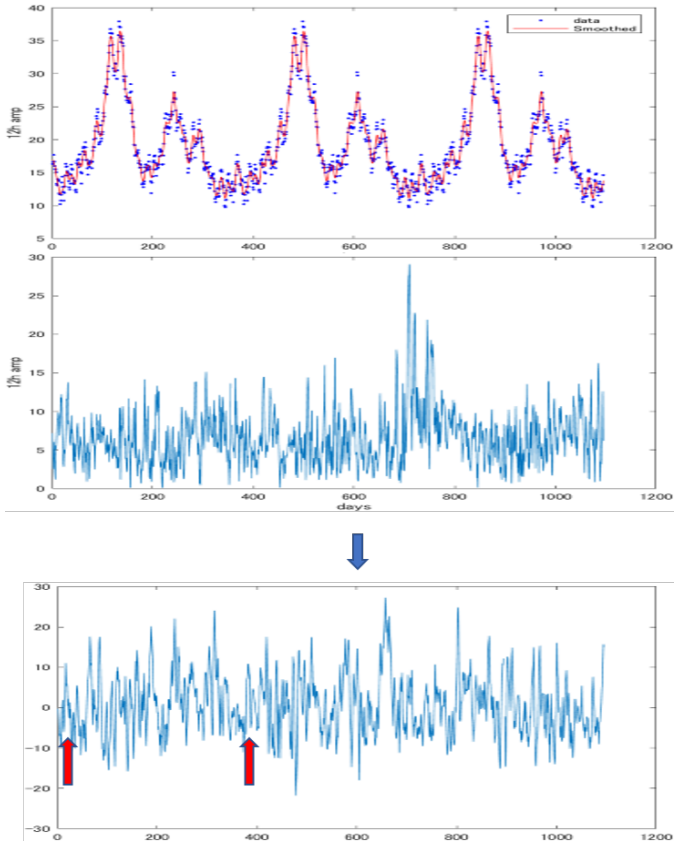

Figure 4.1: An example of Superposed Epoch Analysis procedure of 12h Zonal wind. The figure at the top shows average points and smoothed line, that is, climatology. The figure in the middle shows the raw data. These two are subtracted, and the anomaly at the figure below is obtained. The red arrows show the SSW dates.

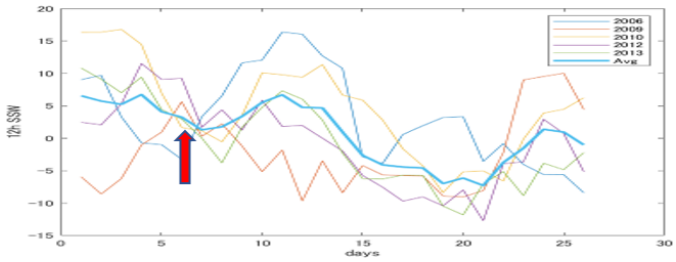

Figure 4.2: All the SSW onset point (red arrow) collected on the same point. The average of before and after the SSW onset will be compared

4.3 Statistical Analysis

Rao and Hibbins et al. [22] has established a statistical analysis method in comparing before and after the magnetic storm, or Dst events. This analysing method was also used in this project both for SSW and Dst events.

4.3.1 Dst

Since the Dst onset dates have hourly information, an hourly climatology was made in order to shift the 4-days segments by one hour at a time instead of one day at a time. Then the hourly anomaly was calculated in the same method as described earlier. The average value of all the data from six days before the Dst onsets to two days before the onset and the average value of the data from two days after the Dst onset to six days after the onset was compared. From two days before the onset and to two days after the onset was not used to make sure that there is a clear seperation between before and after Dst onset. This is because the fitting routine in this project uses 4 days segments and when the range is overlapping before and after the onset date, both before and after the Dst onset is used for curve fitting. The average anomaly for before and after the event was subtracted as explained in superposed epoch analysis, and the statistical significance was calculated by dividing the absolute value of the difference by standard deviation.

4.3.2 SSW

Daily climatology and hourly anomaly was used for statistical analysis for SSW onsets. This time, the three different time frames were defined as:

- Before: from six days before to two days after onset
- After: from two days after to eight days after onset
- Very After: from twelve days after to fifteen days after onset

and the average of the anomaly in each time frame was calculated. These dates were chosen as in Hibbins et al. (2019) paper, and there was a significant negative response of SDT five to six days after the SSW onset followed by a positive enhancement that peaks around thirteen days after the SSW onset in the northern hemisphere [11]. The average anomaly for ”Before”/”After” and ”Before”/”Very After” the event was subtracted, and the statistical significance was calculated by dividing the absolute value of the difference by the standard deviation.

Chapter 5

Results and Discussion

In this chapter, the results using the analysis method described in chapter 4 to the data from Rothera Meteor Radar is shown and discussed.

5.1 Climatology in Rothera

Climatology calculation was conducted to the data from February 2005 to August 2019. Contour plots of the amplitudes of the zonal and meridional components of the Mean, 48h, 24h, 12h and 8h fitted waves from 82km to 98km altitude is shown in Figure 5.1.
Zonal mean wind component shows a robust eastward wind in the winter and westward in the summer at the lowest altitude, which is expected from the sunlight heating the ozone. The result agrees excellently with the earlier study by Hibbins et al. (2006) deriving climatology in Halley, Antarctica. [23] The notable difference is that the altitude of northward wind enhancement in the summer is lower than that of Halley.
For the 24h wind amplitude, both zonal and meridional amplitudes increase with altitude, and the lowest region is in the winter months at the lowest altitudes. The zonal 24h wind shows a maximum at equinox, and the meridional 24h wind has a winter minimum and a summer maximum, which also supports the result from Hibbins et at (2006). [23] The 12h wave amplitude is generally more potent than that of the 24h. Both zonal and meridional wind shows an enhancement around the equinoxes, but the autumn equinox has a more vital enhancement. According to another study by Hibbins et al. (2007) [24], various studies show that for the 12h wave, there is a strong, repeatable autumn enhancement at a high latitude which is associated with a shortening of the vertical scale of the 12h wave consistent with the refraction of the horizontal background flow. The result of this project shows another evidence of an enhancement of the 12h wave in late autumn at Rothera. As Hibbins et al. states, the 12h wave at Rothera is likely a complex mixture of migrating and non-migrating tidal modes.
Hibbins has also stated that Youger et al. [25] have observed the 8h wave in the Northern hemisphere at a similar latitude and altitude, and the amplitude of the wave is seen to increase with altitude, and a maximum in the amplitudes of more than 6m/s is observed at

the highest altitudes around the autumn equinox. This can also be seen in the result from this project, and since the timing of the 8h wave enhancement corresponds with that of 12h and 24h wave enhancement, it supports the theory that the 8h wind us a non-linear interaction between the 12 and 24h waves.

5.2 2-days wave

In the 48h wind climatology in Figure 5.1, there is a substantial enhancement at around day 50 of the year. This matches with the result by Baugaertner et al. (2008) [26] who measured the wind at Rothera and Davis by MFSA radar and showed an oscillation with a period of approximately two days during late January and early February 2005. They state that vertical and horizontal shear of the zonal wind, which can create baroclinic and barotropic instabilities, respectively, were studied and proposed that there is a relationship QTDW. In this study, this 48h wave enhancement was analysed further, as shown in Figure 5.2. The figure in the left side is a reversed climatology of the 48h zonal wind so that the enhancement is centred, and the black line is the 0-wind contour of the background wind. The figure in the right is the wind shear ($\frac{dU}{dz}$) of the zonal background wind. The figures show that after the drop of the 0-wind line, the 2-days wave enhances. The wind shear shows an enhancement before the 48h wave increases and drops after. This provides the obeservational evidence to the idea by Orsolini and Limpasuvan et al. (1997) [27] that the wind shear enhancement causes the QTDW.

5.3 Reaction to Sudden Stratospheric Warming

In this project, the SSW dates based on the criteria established by Stray, Orsolini, et al. (2015) was used [28]. Our group has focused on so called elevated-stratopause events [29]. The conditions for the SSW dates chosen are:

1. The wintertime polar cap (70°N to 90°N) averaged temperature drops below $190K$ between 80 and 100 km

2. The polar cap zonal mean wind reverses from eastward to westward at $1hPa$ (at around 50km) and persists for longer than 5 days [30]

3. The polar cap stratopause altitude changes at least 10 km upward

The SSW onset days were taken from Hibbins et al. (2019), and there were six SSW onset dates which span the period between February 2005 and August 2019. The SSW onset dates used are shown in Table 5.1. Onset date 21 January 2009 is categorized as vortex spilt events and the others as vortex displacement events. [11]
The middle atmosphere circulation moves from the tropics to both poles in the stratosphere, and from the summer pole to the winter pole in the middle atmosphere. Recent studies have suggested that atmospheric conditions at remote locations may be connected by this mesosphere general circulation. In order to investigate the interhemispheric coupling, superposed epoch analysis of the amplitudes of atmospheric waves was performed

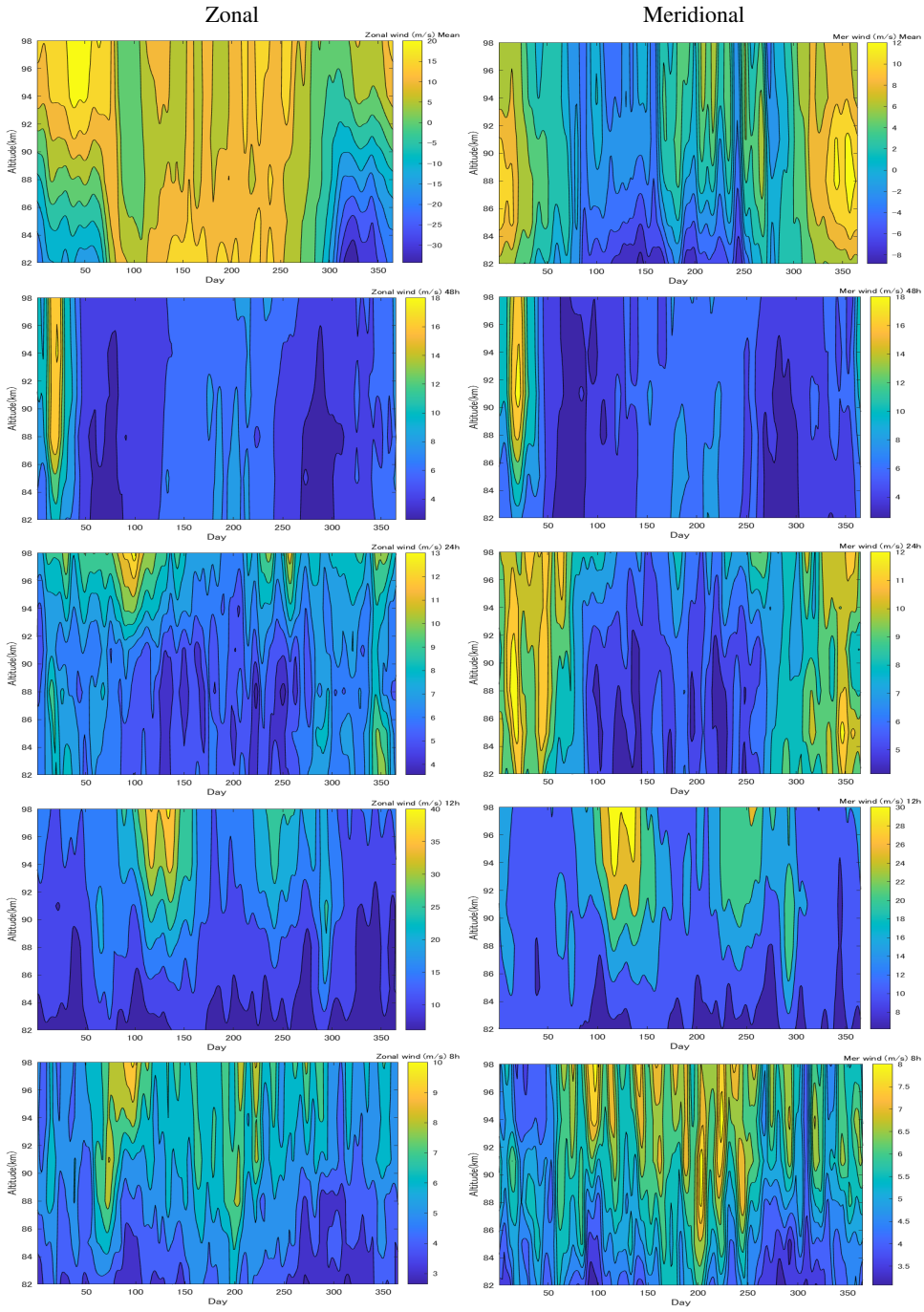

Figure 5.1: Climatology of the Amplitude of Rothera station from February 2005 to August 2019. From the top, Mean wind, 2-days PW, diurnal tide, semidiurnal tide, and terdiurnal tide.

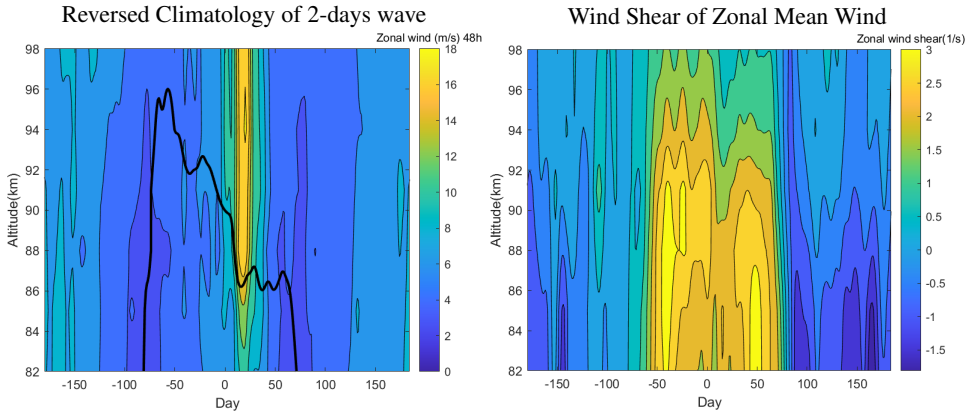

Figure 5.2: Reversed climatology of Zonal 2-days wave (Left) and the Wind Shear(Right). The black line in the climatology is the 0-wind contour of the Zonal Mean wind.

year	month	day
2006	1	8
2009	1	21
2010	1	22
2012	1	13
2013	1	8
2016	3	5

Table 5.1: The list of dates of SSW onsets used for analysis

around the SSW dates in this period.
Results of the superposed epoch analysis are given in Figure 5.3. The full spaghetti-plots are given in the Appendix, Figure A.1, A.2, A.3, A.4, and A.5. From the result, one can see that there is a drop in after the SSW onset for 12h wave and a slight enhancement after the onset for 48h wave. This is consistent in the spaghetti plots as well. A statistical analysis described in Chapter 4 was conducted as well. Figure 5.4 shows the statistical analysis around SSW for 12h and 48h wind. The left column shows the anomaly, the data subtracted by the climatology. ”Before” is the average value of the period from 6 days before the onset to 2 days before the onset, ”After” is that from 2 days after to 8 days after onset, and ”Very After” is from 12 to 15 days after. The middle column shows the difference between before and after/very after the event. The right column shows the statistical significance of the difference, which is the absolute value of the difference divided by the standard deviation.
The results show high statistical significance in both zonal and meridional wind of 12h tides. For the 48h tides, the statistical significance is slightly high at 88km altitude. According to Hibbins et al. (2019), there is a significant negative response of SDT 5 or 6 days after the SSW onset followed by a positive enhancement that peaks around 13 days

after the SSW onset in the northern hemisphere [11]. The result at Rothera, southern hemisphere, shows that there is a remarkable drop in the amplitude of 12h waves from 12 to 15 days after the onset, which is the opposite reaction than in the Northern hemisphere. This result matches with the work of WACCM-X calculations during SSW done by Zhang, Limpasuvan, Orsolini et al. (under review) [9] which simulates the SSW response in the Southern hemisphere. SW2 (the major mode of the semidiurnal tide) amplitude is presented by the group as in Figure 5.6. The northern hemisphere is characterised in this calculation by a decrease in the semidiurnal tide (SDT) followed by an increase, which matches the observational result by Hibbins et al. (2019) [11]. However, Zhang et al. have predicted an opposite effect in the southern hemisphere, where there first is seen an increase in the SDT followed by a decrease, and this is observationally shown in this thesis. The reasons for this opposite behaviour is described to be the propagation of the tide from its source region in the equatorial stratosphere through the northern hemisphere winter and southern hemisphere summer wind regimes, where winter wind is predominantly eastward and summer wind is predominantly westward

The slight increase of the amplitude of the 48h wind is similar to the result by Stray et al. (2015) [28], where the group investigated the effect of SSW on PW activity in the MLT in the Northern hemisphere. They claim that the enhancement of the PW activity in the MLT is a general feature connected to SSWs in the Northern Hemisphere. The result of this project indicates that there might be a slight enhancement after the onset. However, the statistical significance is not that high. Further analysis can be done by changing the time frame of ”After” and ”Very After” to see whether it will show clearer enhancement after the SSW onset.

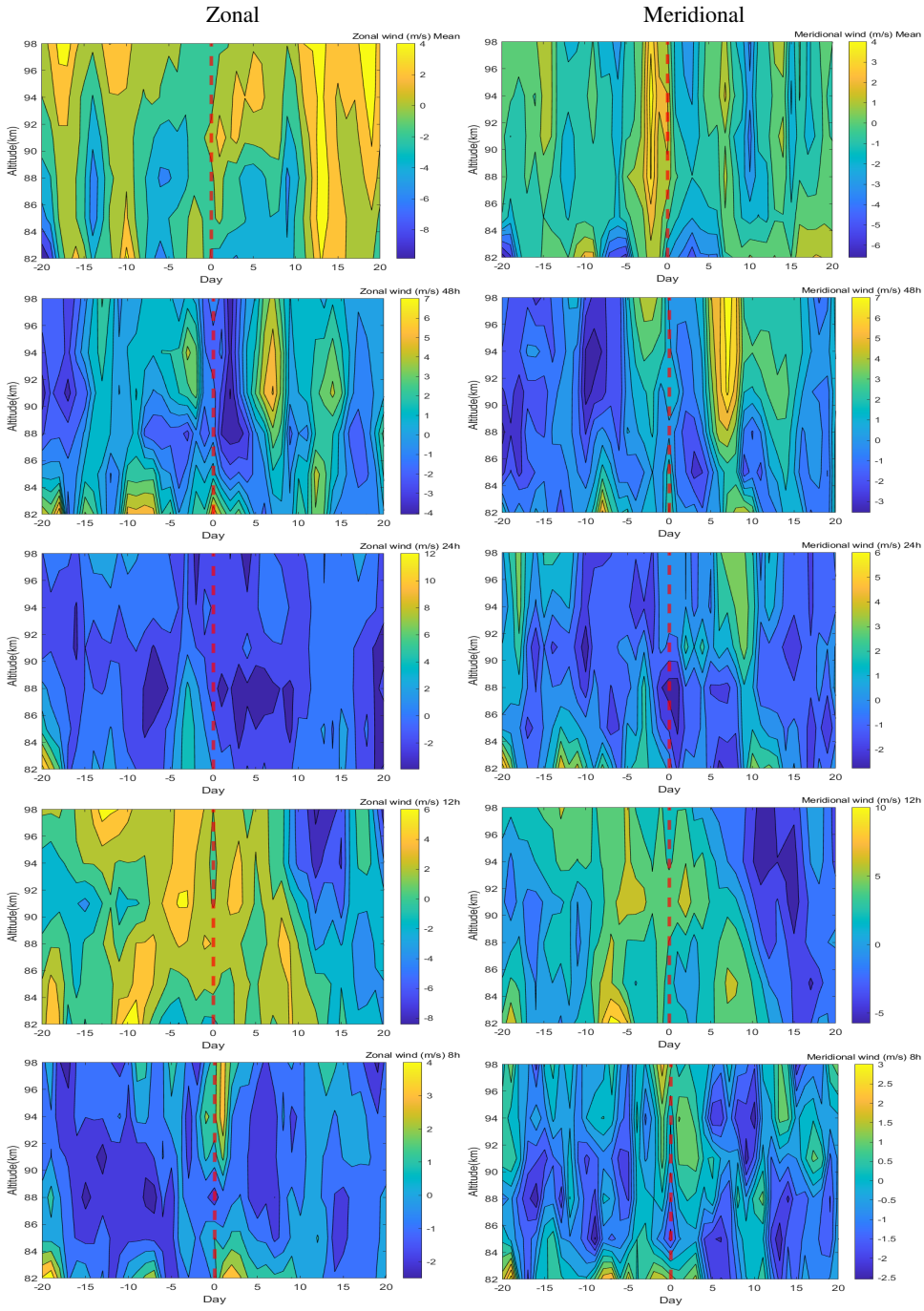

Figure 5.3: Superposed Epoch Analysis around SSW onset (red line) of Rothera station. From the top, Mean wind, 2-days PW, diurnal tide, semidiurnal tide, and terdiurnal tide.

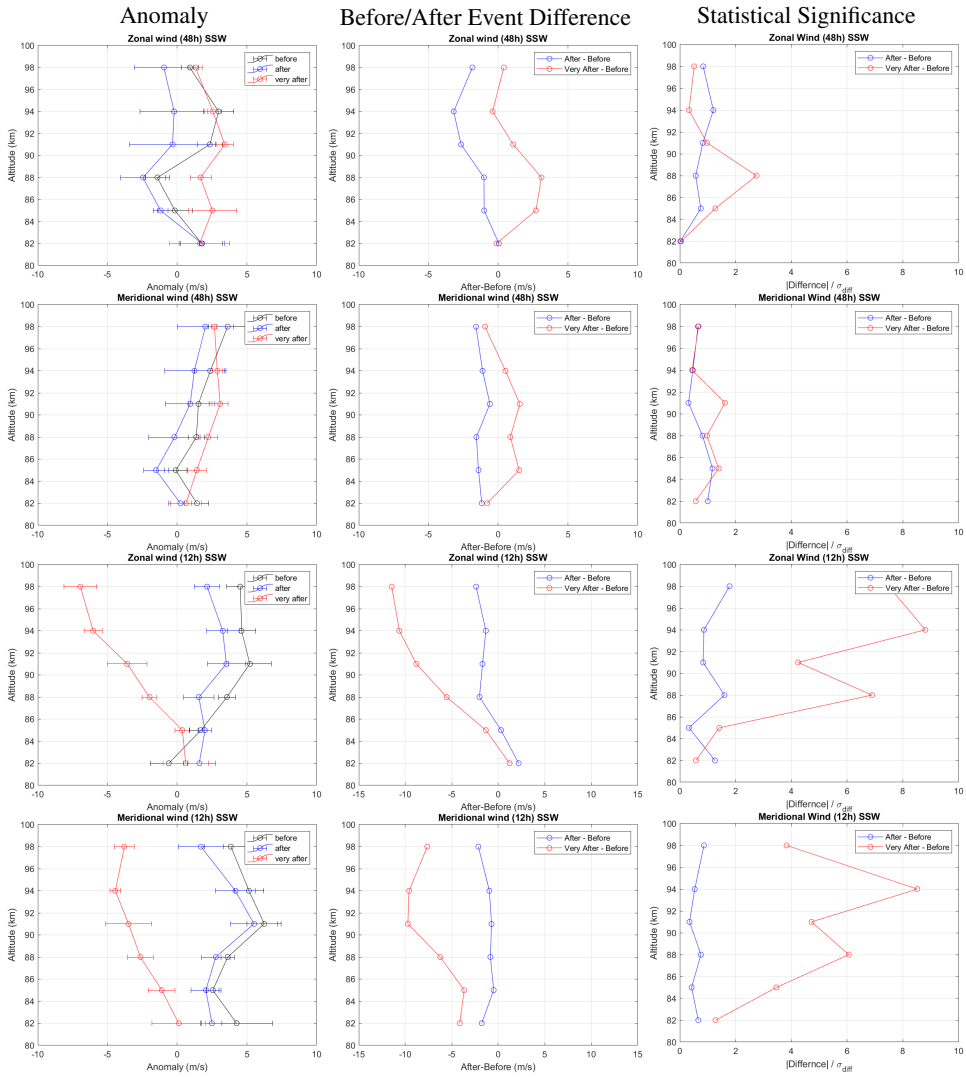

Figure 5.4: Statistical analysis using Hibbins-method around SSW onset of Rothera station. From the top, 48h zonal, 48h meridional, 12h zonal, and 12h meridional tide amplitude

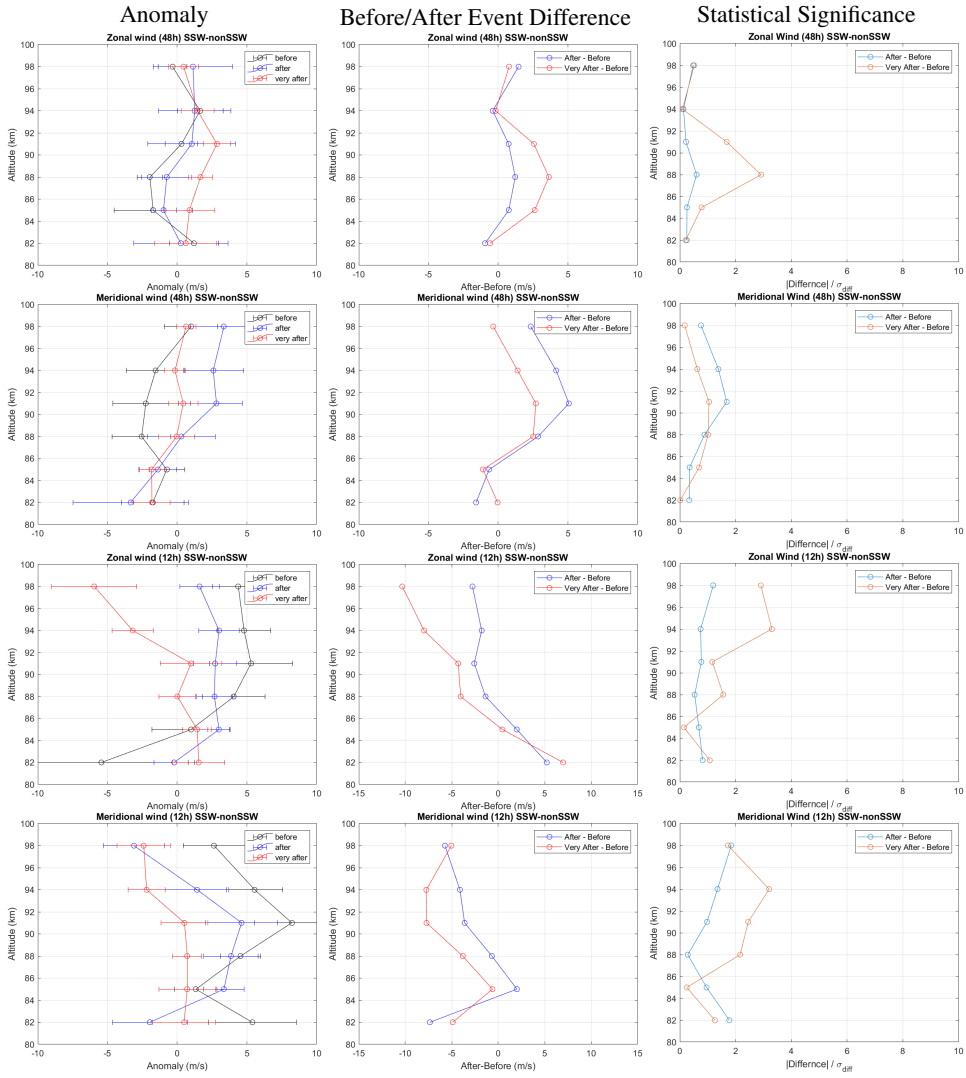

Figure 5.5: Subtraction of random non-SSW onset from SSW onset for the Statistical analysis of Rothera station. From the top, 48h zonal, 48h meridional, 12h zonal, and 12h meridional tide amplitude

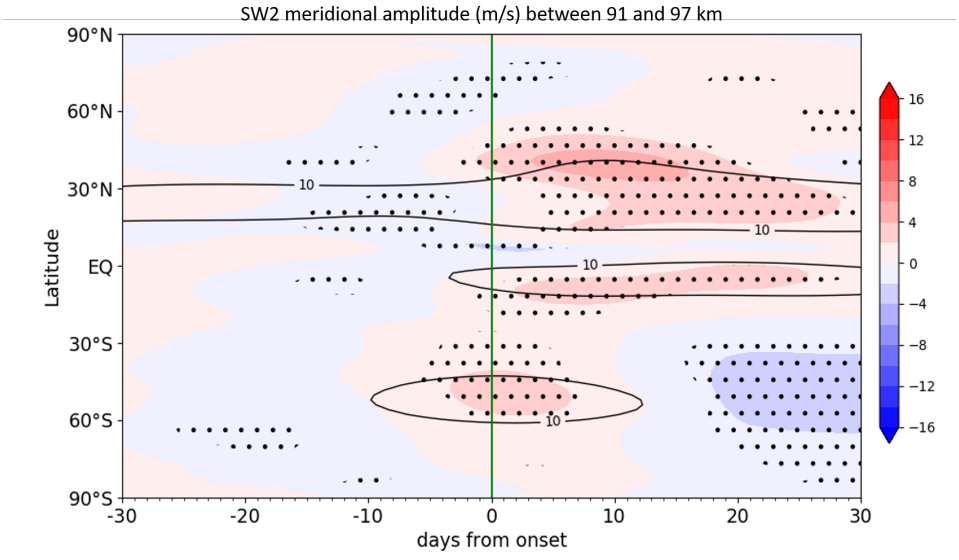

Figure 5.6: SW2 amplitude during SSW calculated using WACCM-X [9]

Comparison of climatologies in the SSW years and non-SSW years was also conducted and shown in Figures 5.7 and 5.8. The interesting difference between the two climatologies is the difference in wind shear of the mean wind and the level of enhancement in 48h wind. In SSW years, the wind shear of the wind shear in the start of the year is great, and the enhancement of the 48h wind is relatively weak, but in non-SSW years, the wind shear is weak, and the enhancement of the 48h wind is substantial. This can indicate that in SSW years, the wind shear is less likely to enhance the QTDW, and in non-SSW years, the QTDW is more likely to eat up the wind shear.
In the future work, the climatology must be reversed so that the SSW season will be in the centre to see whether the slight enhancement in the 24h wind at the end of the year at lower altitude is significant.

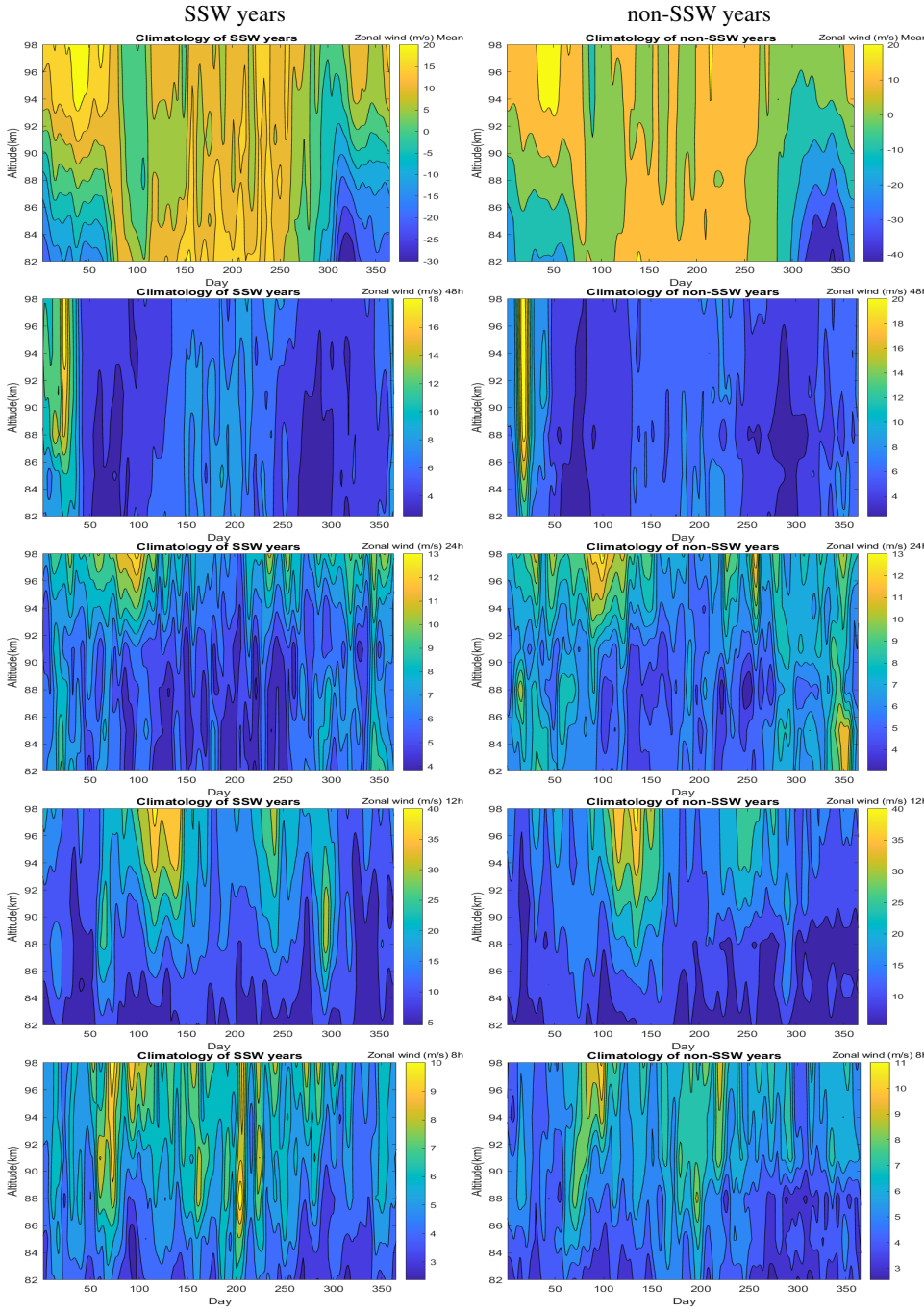

Figure 5.7: Climatology comparison of SSW years and non-SSW years. From the top, Mean, 48h, 24, 12, and 8h Zonal Wind.

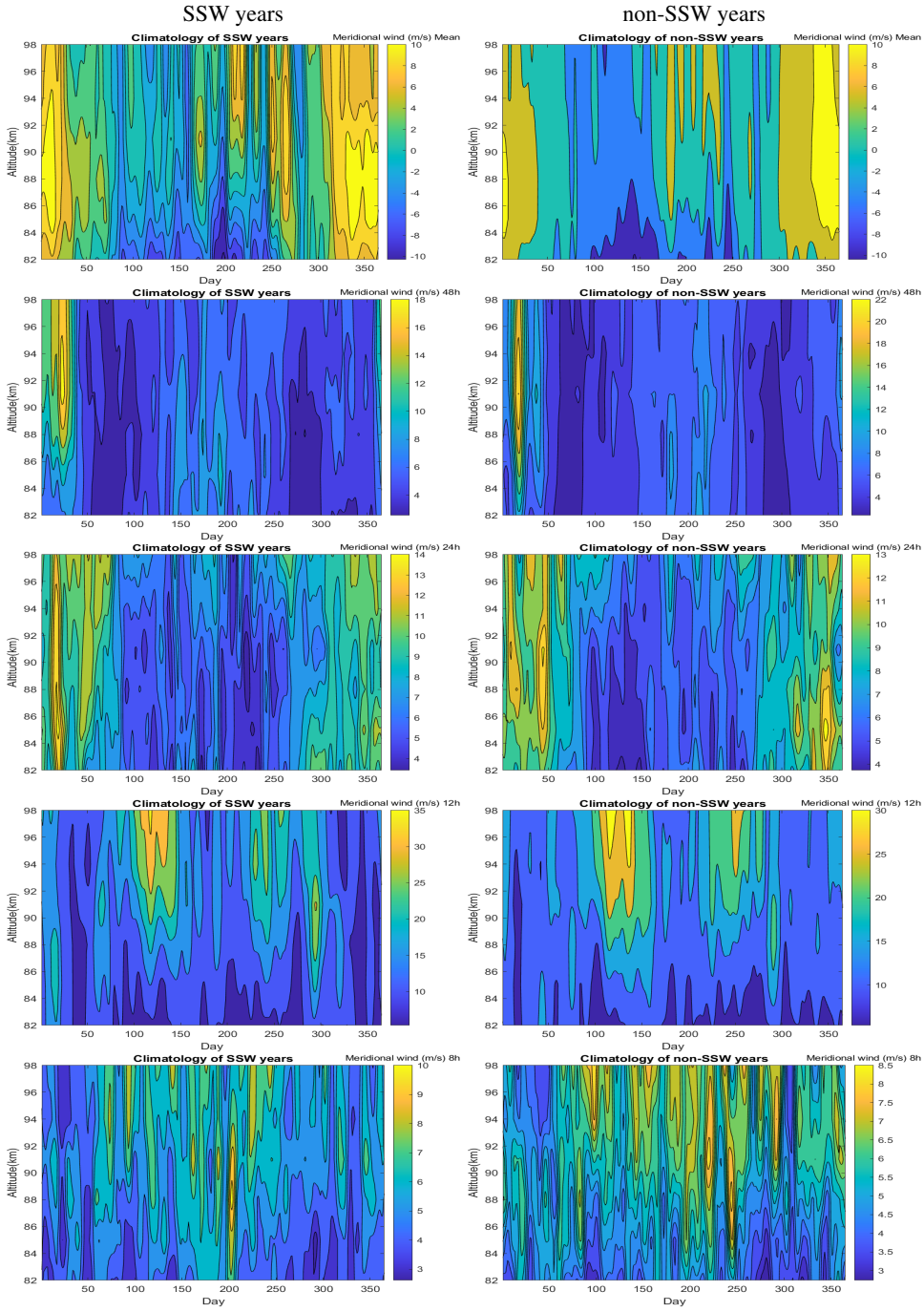

Figure 5.8: Climatology comparison of SSW years and non-SSW years. From the top, Mean, 48h, 24, 12, and 8h Meridional Wind.

5.4 Reaction to Magnetic Storm

Since the method of calculating the climatology and conducting superposed epoch analysis around an event was established, this method can be applied to other events such as a magnetic storm. Rao, Espy, Hibbins et al. (unpublished) [22] has looked into the effect of the magnetic storm to the atmospheric wave components using MF radar at Rothera. Southern hemisphere high latitudes are less variable than in the North, so small changes are easier to detect. The Rothera MF radar [31] [32] operates at 1.98MHz and detects partial reflection scattering from weak ionization in the mesosphere. The scatter occurs most at heights between 75 and 100km and is gated into profiles with an altitude resolution of 4km. Dst index, which is an index that shows the onset of a magnetic storm event, is used, and the date and the hour of the event onset are shown in Table A.1 in the Appendix which the date list is developed by Rao and Hibbins et al. [22]. The plots of the Dst events are shown in Appendix A Fig. A.12. The group has examined the same dates using the MF radar that extends to a lower altitude to about 74km. The same procedure as this group has done in this project with the Meteor Radar data, which provides data in the higher altitude more accurately than the MF radar.
The criterias used by Rao's group in creating the Dst onset dates are:

1. Dst must be transfered from positive to negative.
2. Dst in the previous 96 hours must be greater than -30nT.
3. Dst in the subsequent 24 hours must be smaller than -50nT.
4. Only the events that are at least 168 hours apart are included. If the two events are closer than 168 hours, only the first event is included.

The Statistical analysis in Hibbins-method was performed around the Dst onset. Since the Dst-event onset includes hourly information as well, the 4-days window for the wave-fitting routine was moved 1 hour at a time instead of 1 day at a time. The result of the Hibbins-method analysis around the Dst onset is shown in Figure 5.9 and 5.10. The figures show the statistical analysis around Dst for the atmospheric wave components. The left column shows the anomaly, the data subtracted by the climatology. "Before" is the average value from 6 days to 2 days before the onset, "After" is that from 2 days to 6 days after the onset. The middle column shows the difference between before and after the event. The right column shows the statistical significance of the difference, which is the absolute value of the difference divided by the standard deviation. The result shows that there might be statistically significant enough increase in the mean, 12h, and 24h wind, however, the maximum difference is only around 2σ. This can be considered as a difference within a variation in the atmosphere, since the maximum wind anomaly is around 2m/s and was within the maximum variation by WACCM simulation by Guttu et al. [33]. The group has run the WACCM model with and without particle precipitation to look at the subsequent effects on the dynamics of the chemical changes produced by the particle precipitation. This work showed that the maximum effects occurred in the southern hemisphere in August. The effect of particle precipitation on the zonal winds during August are shown in Figure 5.11 (Orsolini, personal communication), showing that at (68°S and

above 80 km, the wind changes are on the order of 1m/s.

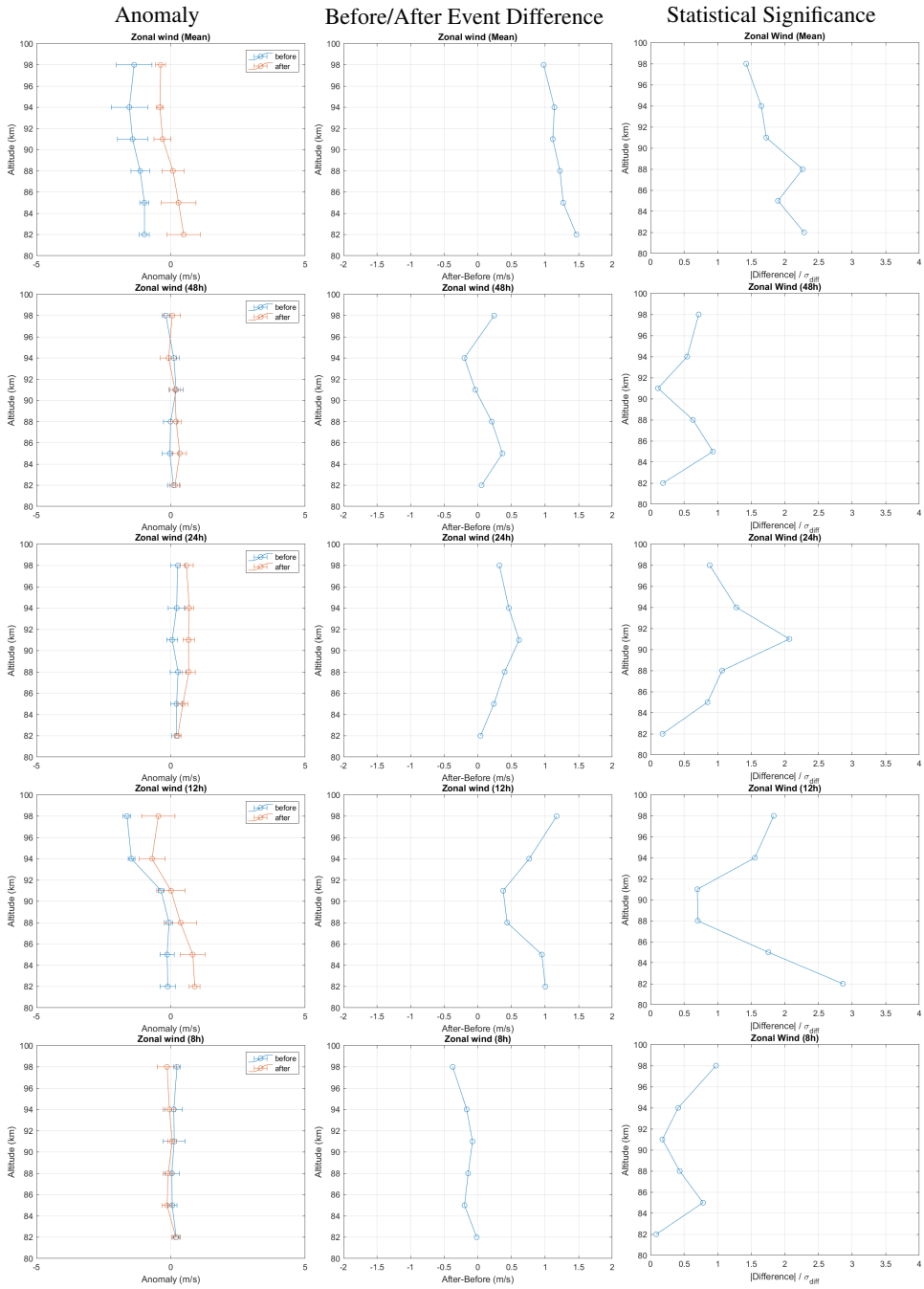

Figure 5.9: Statistical analysis of Dst onset at Rothera station. From the top, Mean, 48h, 24h, 12h, 8h Zonal tide amplitude

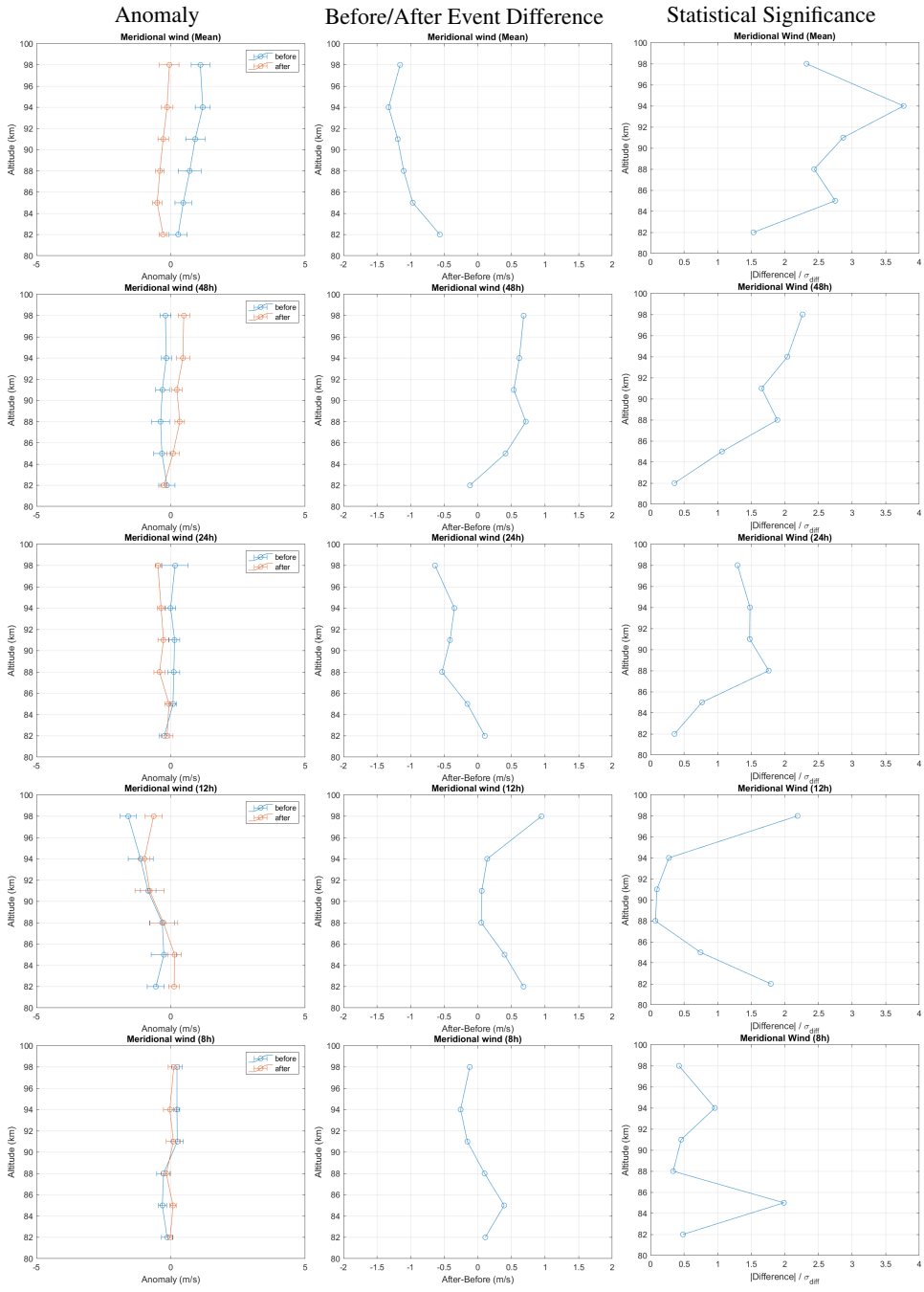

Figure 5.10: Statistical analysis of Dst onset at Rothera station. From the top, Mean, 48h, 24h, 12h, 8h Meridional tide amplitude

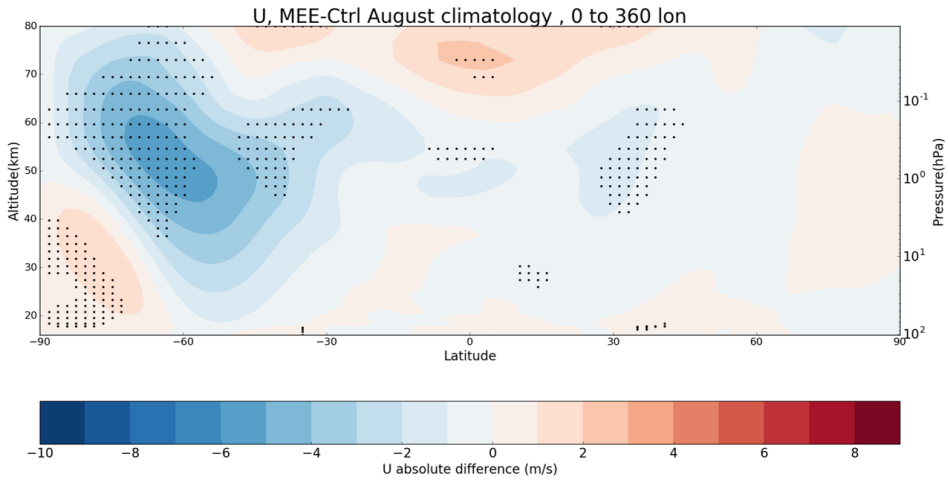

Figure 5.11: The effect of particle precipitation on the zonal winds during August (Orsolini, personal communication)

Chapter 6

Conclusion

Meteor Radar data in Antarctica, Rothera in the period February 2005 to August 2019 was used to obtain the amplitudes of the atmospheric wave components in the polar southern hemisphere. The amplitudes of the atmospheric waves were averaged in each day of the year for the 15 years, and a daily average amplitude pattern, climatology was generated. The climatology showed an agreement with earlier studies that calculated the climatology in the southern hemisphere. The 48h wind amplitude showed a significant enhancement around late January, and early February, so further analysis comparing the timing of the enhancement of the 48h wind amplitude with the wind shear of the mean background wind was conducted. This supports the theory by Stray, Orsolini, Limpasuvan et al. (2015) that the wind shear causes the QTDW.

Based on the climatology of Rothera station, a superposed epoch analysis around the SSW onset days was performed and compared with the earlier analysis of SSW in the northern hemisphere to investigate the interhemispheric coupling. There were drop after the SSW onset in the 12-hours wave amplitude and a slight enhancement after the SSW onset for the 48-hours wave amplitude. For the 12-hours wave, it is the opposite response to that of Hibbins et al. (2019) [11] observed in the Northern hemisphere. This result also has become an observational evidence of the WACCM simulation by Zhang et al. (under review) [9] which showed a simulation of negative response in the southern hemisphere after SSW. The statistical analysing could be done with a different timeframe for ”After” and ”Very after” the event for further analysis to other wave components.

Climatology for SSW years and non-SSW years were created and compared as well. It showed a difference in wind shear and the level of enhancement of the 48h wind in late January to early February. This could indicate that in SSW years, the wind shear is less likely to enhance the QTDW. For the climatology comparison, the climatology could be reversed half a year to include the end of the year before the SSW as a SSW-year.

As an application of the analysing method above, the atmospheric tide reaction to the magnetic storm was conducted. There was a slight enhancement after the storm in the mean, 12h, and 24h with the maximum difference of 2σ. However, this could be considered as a difference within the variation in the atmosphere as calculated by Guttu et al. (2019) [33].

As a future project, it would be interesting to analyse the reaction to SSW in the same method, but in other stations in the southern hemisphere. This could separate the 12h waves into migrating and non-migrating waves.

Bibliography

[1] Nora Kleinknecht. Planetary wave oscillations observed in ozone from troll station antarctica. Master's thesis, 2010.

[2] Gordon Rostoker. Geomagnetic indices. *Review of Geophysics and Space Physics*, 10(4):935–950, 1972.

[3] Data analysis center for geomagnetism and space magnetism, kyoto university. `http://wdc.kugi.kyoto-u.ac.jp/dstdir/index-j.html`. Accessed: 2020-September.

[4] Nptel atmospheric science. `https://nptel.ac.in/courses/119/102/119102007/`. Accessed: 2020-09-01.

[5] John W. Meriwether and Andrew J. Gerranrd. Mesosphere inversion layers and stratosphere temperature enhancements. *Rev. Geophys.*, 42, 2004.

[6] Kjetil Landgraff Ekern. Climatology of short-period tidal oscillations in the upper atmosphere. Master's thesis, 2013.

[7] J. P. Eastwood, H. Hietala, and Phan T. D. Fujimoto M. Toth, G. What controls the structure and dynamics of earth's magnetosphere? *Space Sci Rev*, 188:251–286, 2015.

[8] Atmospheric group webpage. `https://home.phys.ntnu.no/brukdef/prosjekter/atmosfys/web-pages/SKiYMET-wind.php`, note = Accessed: 2020-September.

[9] Jiarong Zhang, Var Limpasuvan, Yvan Orsolini, Patrick J. Espy, and Robert E Hibbins. Climatological westward-propagating semidiurnal tides and their composite response to sudden stratospheric warming in superdarn and sd-waccm-x. Under Review.

[10] Rosmarie J. de Wit. *Quantifying the influence of the stratosphere on the mesosphere and lower thermosphere*. PhD thesis, 2014.

[11] R. E. Hibbins, P. J. Espy, Y. J. Orsolini, V. Limpasuvan, and R. J. Barnes. Superdarn observations of semidiurnal tidal variability in the mlt and the responce to sudden stratospheric warming events. *J. Geophys. Res. Atmos.*, 124:4862–4872, 2019.

[12] Nora H. Kleinknecht, Patrick J. Espy, and Robert E. Hibbins. The climatology of zonal wave numbers 1 and 2 planetary wave structure in the mlt using a chain of northern hemisphere superdarn radars. *J. Geophys. Res. Atmos.*, 119:1292–1307, 2014.

[13] David G. Andrews. *An Introduction to Atmospheric Physics Second Edition*. Cambridge University Press, 2010.

[14] Tokyo university sato group webpage. `http://www-aos.eps.s.u-tokyo.ac.jp/~sato-lab/`. Accessed: 2020-September.

[15] Nora H. Stray. *Planetary waves in the northern MLT: Vertical coupling and effects*. PhD thesis, 2015.

[16] Jeffrey M. Forbes. Vertical coupling by the semidiurnal tide in earth's atmosphere. *Climate and Weather of the Sun-Earth System (CAWSES)*, 2009.

[17] Elise Wright Knutsen. Dynamical-chemical coupling in the polar middle atmosphere. Master's thesis, 2019.

[18] W. K. Hocking, B. Fuller, and B. Vandepeer. Real-time determination of meteor-related parameters utilizing modern digital technology. *Journal of Atmospheric and Solar-Terrestrial Physics*, 63:155–169, 2001.

[19] W. K. Hocking. Temperatures using radar-meteor decay times. *Geophysical Research Letters*, 26(21):3297–3300, 1999.

[20] B. A. Laken and J. Calgovic. Composite analysis with monte carlo methods: an example with cosmic rays and clouds. *J. Space Weather Space Clim.*, 3, 2013.

[21] S. E. Forbush, M. A. Pomerantz, S. P. Duggal, and C. H. Tsao. Statistical consderation in the analysis of solar oscillation data by the superposed epoch method. 1983.

[22] N. Venkateswara Rao, Patrick Espy, and Rob Hibbins. Energetic particle precipitation effects on the dynamics of mesosphere and lower thermosphere over rothera. Unpublished.

[23] R. E. Hibbins, P. J. Espy, and M. J. Jarvis. Mean winds and tides in the mesosphere and lower thermosphere above halley, antarctica. *Journal of Atmospheric and Solar-Terrestrial Physics*, 68:436–444, 2006.

[24] R. E. Hibbins, P. J. Espy, M. J. Jarvis, D. M. Riggin, and D. C. Fritts. A climatology of tides and gravity wave variance in the mlt above rothera, antarctica obtained by mf radar. *Journal of Atmospheric and Solar-Terrestrial Physics*, 69:578–588, 2007.

[25] P. T. Younger, D. Pancheva, H. R. Middleton, and N. J. Mitchell. The 8-hour tide in the arctic mesosphere and lower thermosphere. *Journal of Geophysical Research*, 107(A12), 2002.

[26] A. J. G. Baumgaertner, A. J. McDonald, R. E. Hibbins, and D. C. Fritts. Short-period planetary waves in the antarctic middle atmosphere. *Jounal of Atmospheric and Solar-Terrestrial Physics*, 70:1336–1350, 2008.

[27] Y. J. Orsolini, V. Limpasuvan, and C. B. Leovy. The tropical stratopause in the ukmo stratospheric analyses: evidence for a 2-day wave and inertial circulations. *Quarterly Journal of the Royal Meteorological Society*, 123(542):1701–1724, 1997.

[28] N. H. Stray, Y. J. Orsolini, P. J. Espy, V. Limpasuvan, and R. E. Hibbins. Observations of planetary waves in the mesosphere-lower thermosphere during stratospheric warming events. *Atmos. Chem. Phys.*, 15:4997–5005, 2015.

[29] Amy H. Butler, Dian J. Seidel, Steven C. Hardiman, Neal Butchart, Thomas Birner, and Aaron Match. Defining sudden stratospheric warmings. *Bull. Amer. Meteor. Soc.*, 96:1913–1928, 2015.

[30] O. V. Tweedy, V. Limpasuvan, Y. J. Orsolini, A. K. Smith, R. R. Garcia, D. Kinnison, C. E. Randall, O. K. Kvissel, F. Stordal, V. L. Harvey, and A. Chandran. Nighttime secondary ozone layer during major stratospheric sudden warming in specified-dynamics waccm. *J. Geophys. Res. Atmos.*, 118:8346–8358, 2013.

[31] M. J. Jarvis, G. O. L. Jones, and B. Jenkins. New initiatives in observing the antarctic mesosphere. *Advances in Space Research*, 24(5):611–619, 1999.

[32] P. J. Espy, R. E. Hibbins, and G. O. L. Jones. Rapid, large-scale temperature changes in the polar mesosphere and their relationship to meridional flows. *Geophysical Research Letters*, 30(5), 2003.

[33] Sigmund Guttu, Yvan Orsolini, Frode Stordal, Varavut Limpasuvan, and Daniel R. Marsh. Waccm simulations: Decadal winter-to-spring climate impact on middle atmosphere and troposphere from medium energy electron presipitation. *Jounal of Atmospheric and Solar-Terrestrial Physics*, 2019.

Appendix A

Figures

A.1 SSW Analysis

The spaghetti plots and the Hibbins-method statistical analysis around the SSW onset are shown.

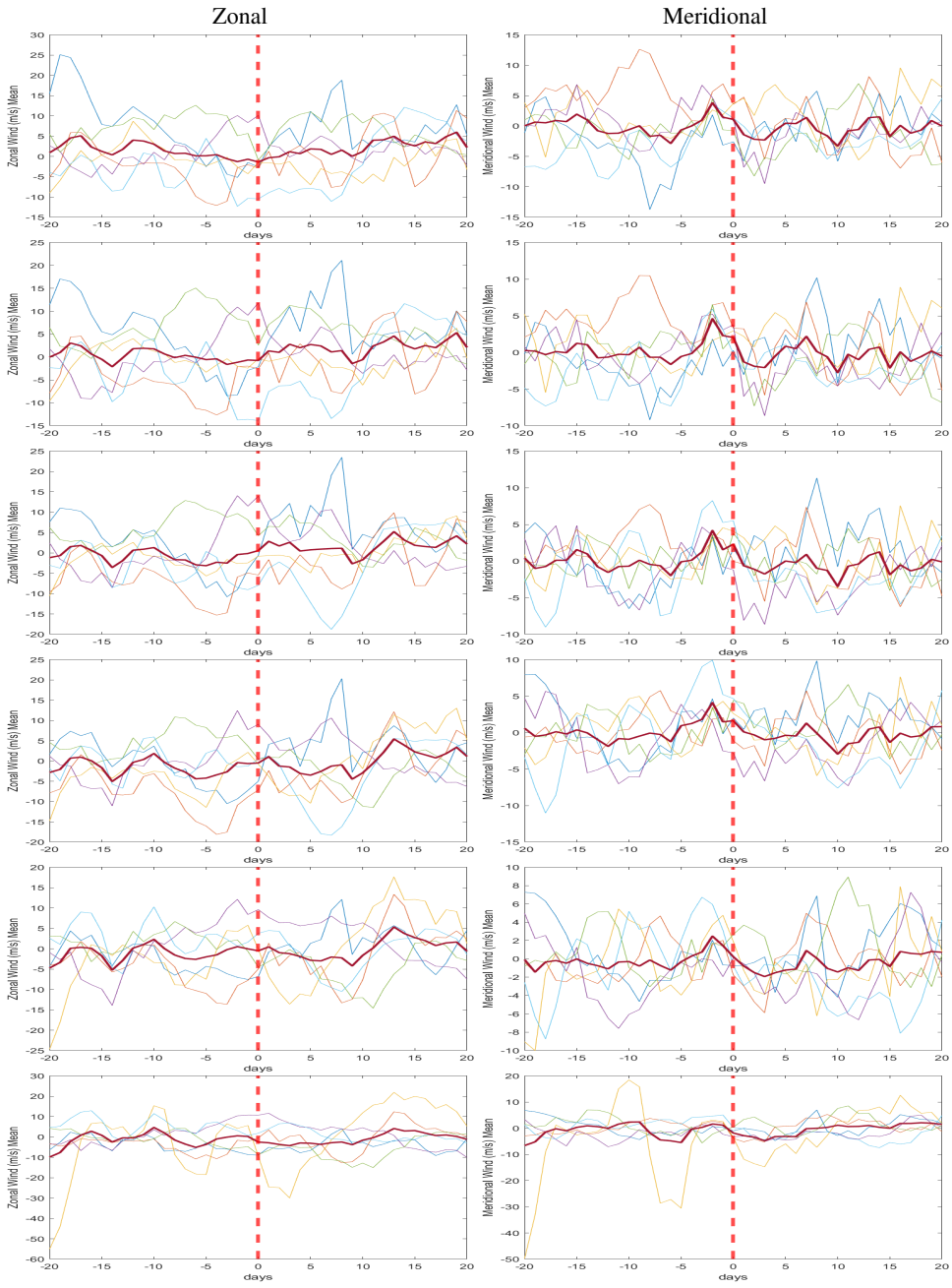

Figure A.1: Spaghetti-plots of Mean wind Superposed Epoch Analysis around SSW onset (red line) of Rothera station. From the top, 98km, 95km, 91km, 88km, 85km, 82km

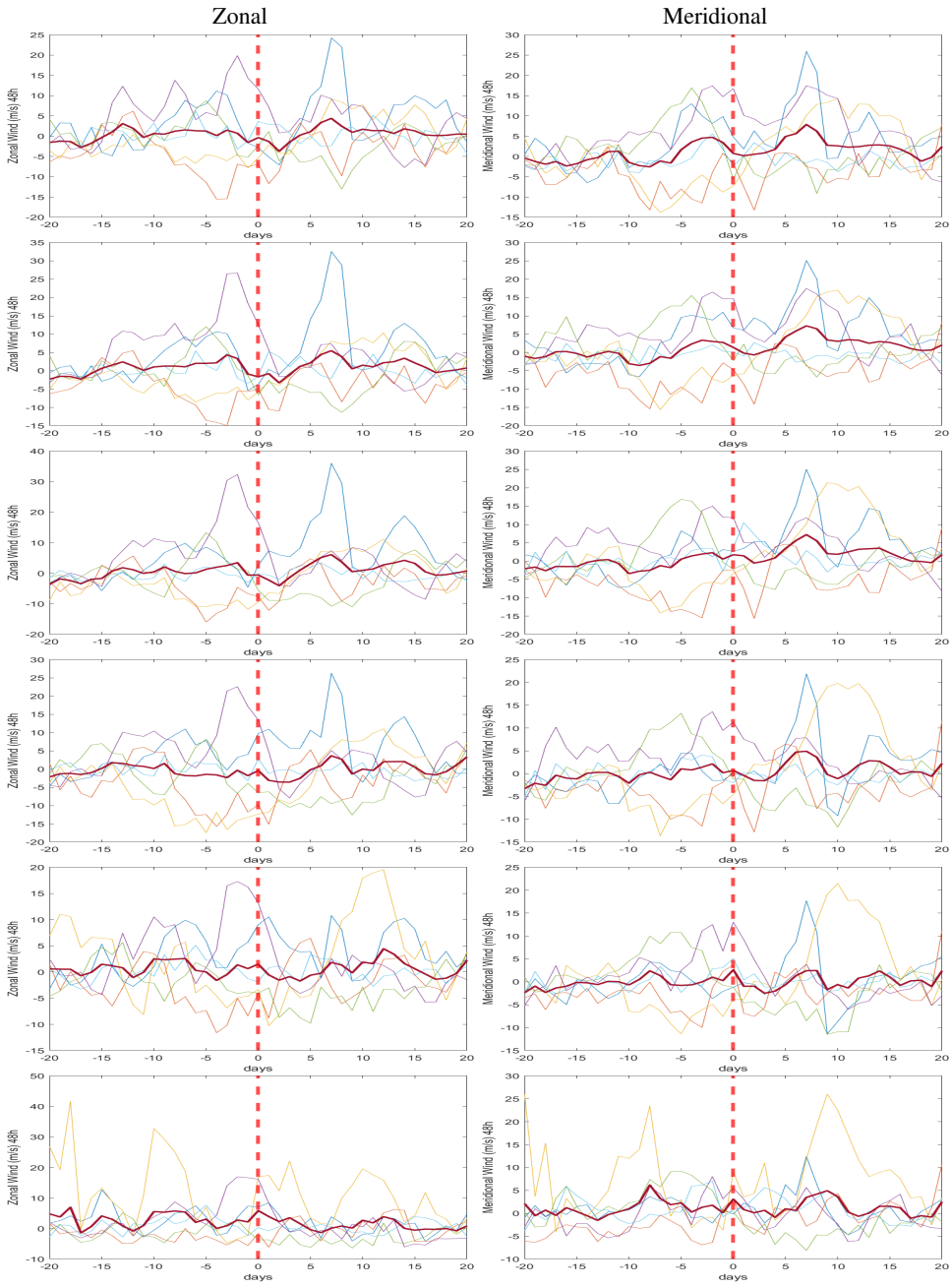

Figure A.2: Spaghetti-plots of 48h wind Superposed Epoch Analysis around SSW onset (red line) of Rothera station. From the top, 98km, 95km, 91km, 88km, 85km, 82km

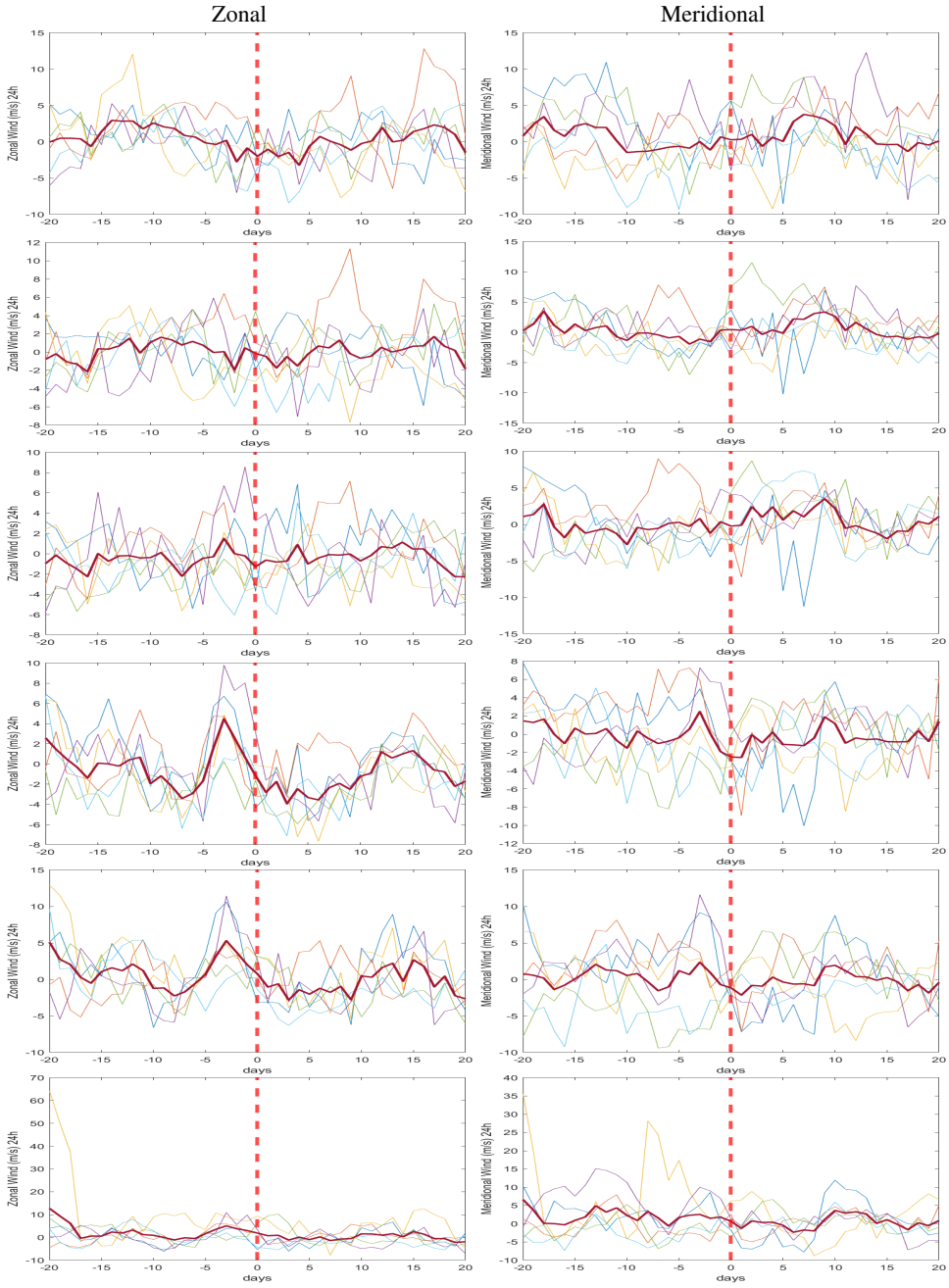

Figure A.3: Spaghetti-plots of 24h wind Superposed Epoch Analysis around SSW onset (red line) of Rothera station. From the top, 98km, 95km, 91km, 88km, 85km, 82km

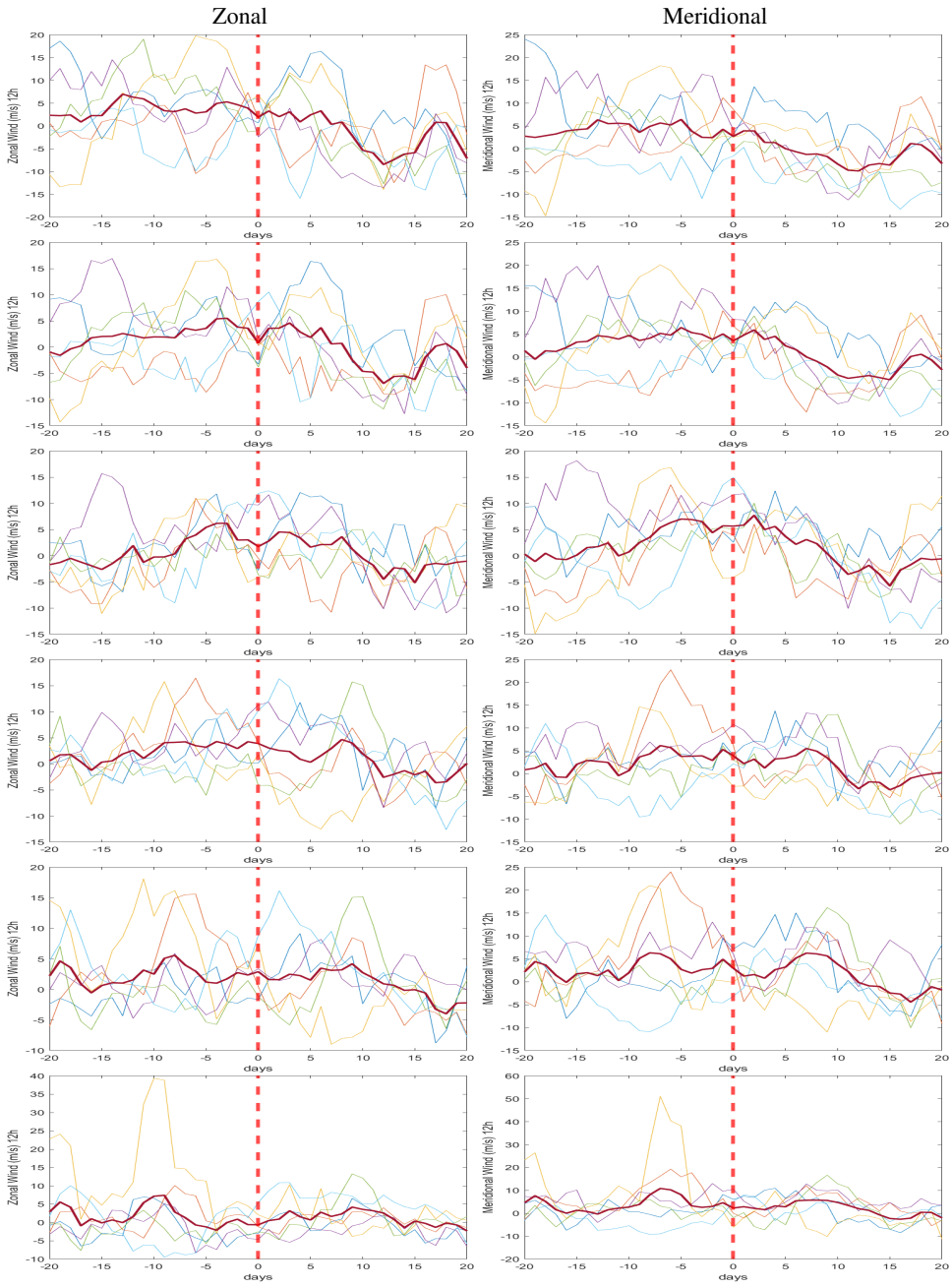

Figure A.4: Spaghetti-plots of 12h wind Superposed Epoch Analysis around SSW onset (red line) of Rothera station. From the top, 98km, 95km, 91km, 88km, 85km, 82km

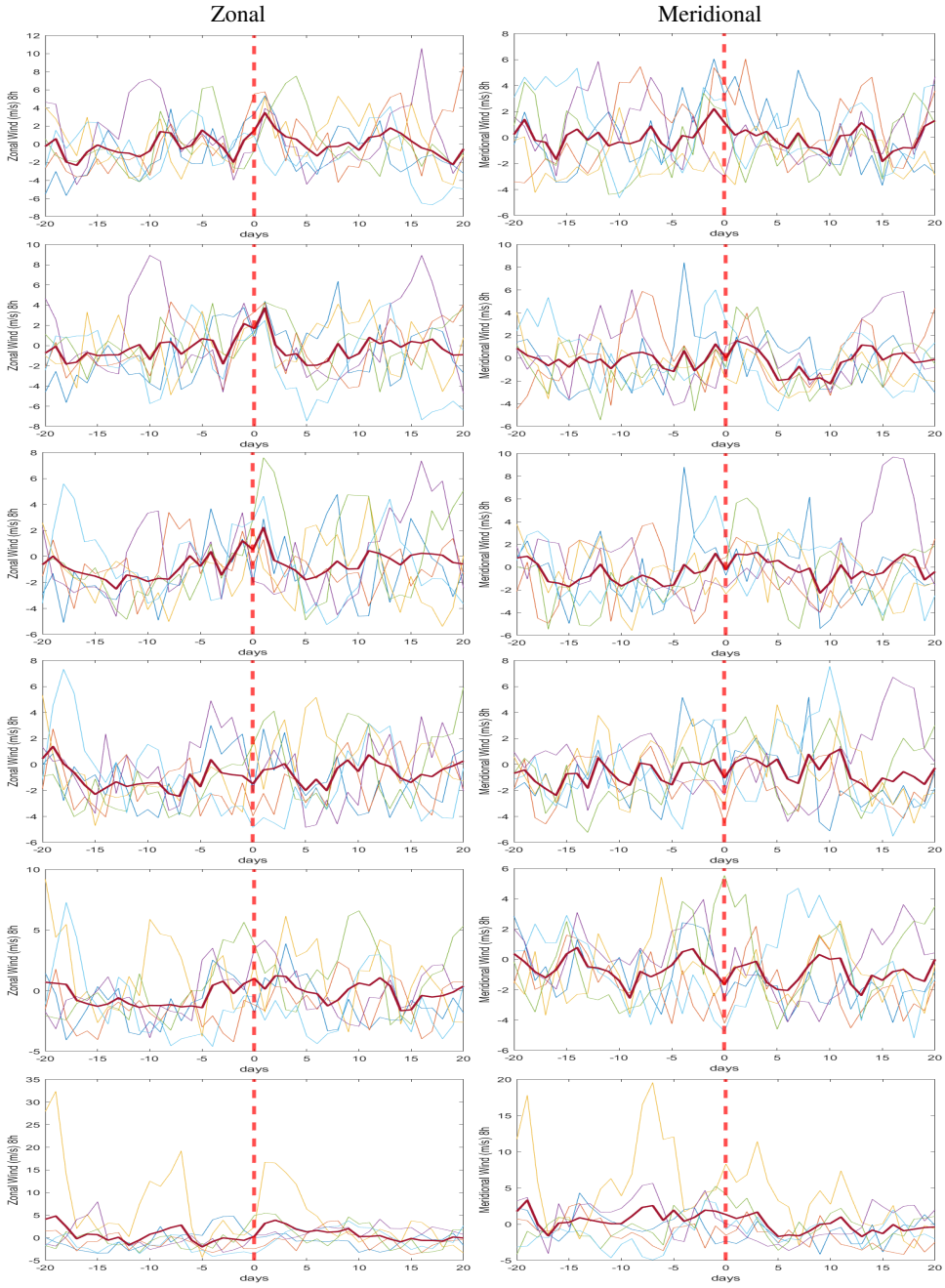

Figure A.5: Spaghetti-plots of 8h wind Superposed Epoch Analysis around SSW onset (red line) of Rothera station. From the top, 98km, 95km, 91km, 88km, 85km, 82km

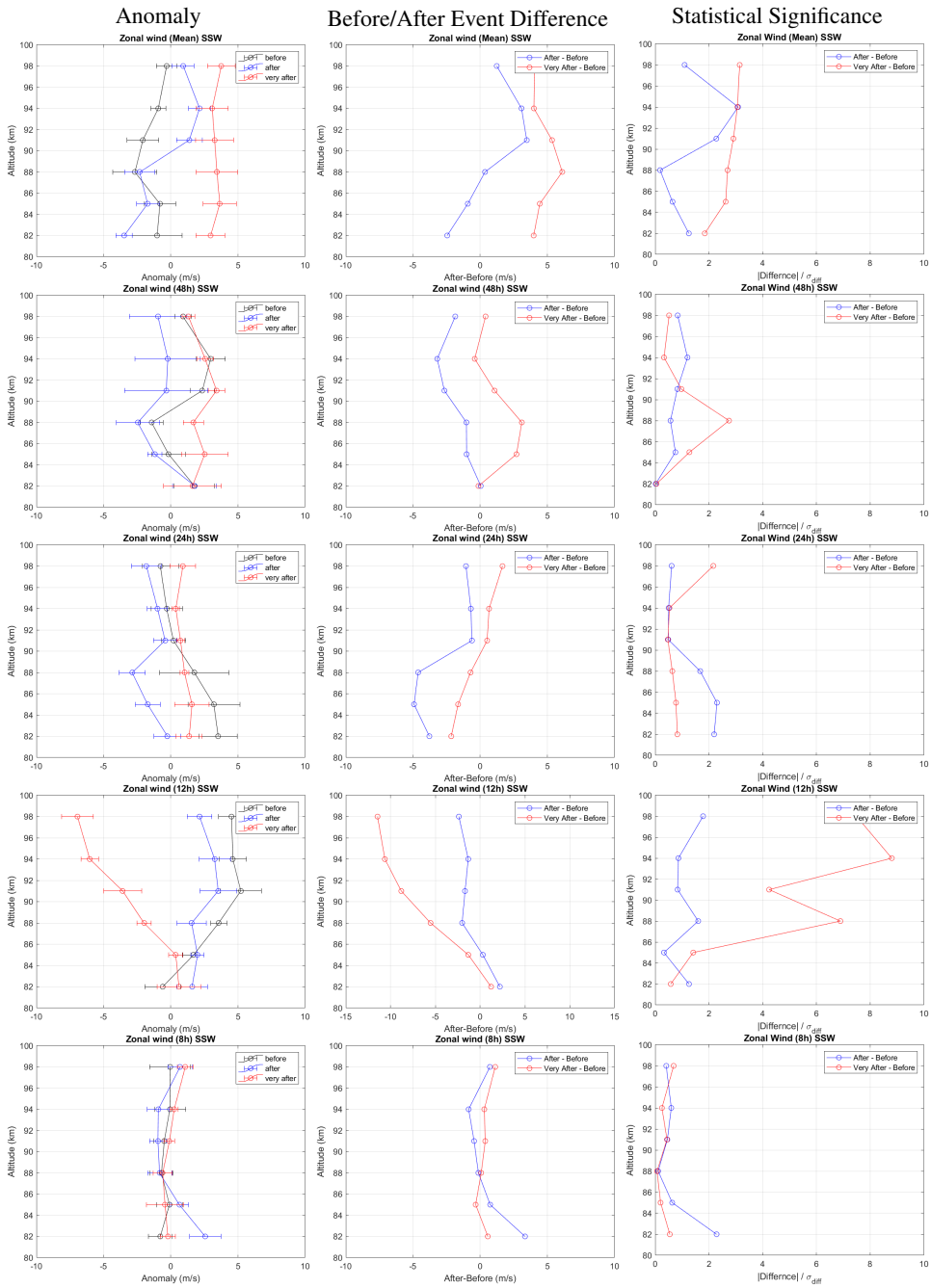

Figure A.6: Statistical analysis using Hibbins-method around SSW onset of Rothera station. From the top, Mean, 48h, 24h, 12h, 8h zonal tide amplitude

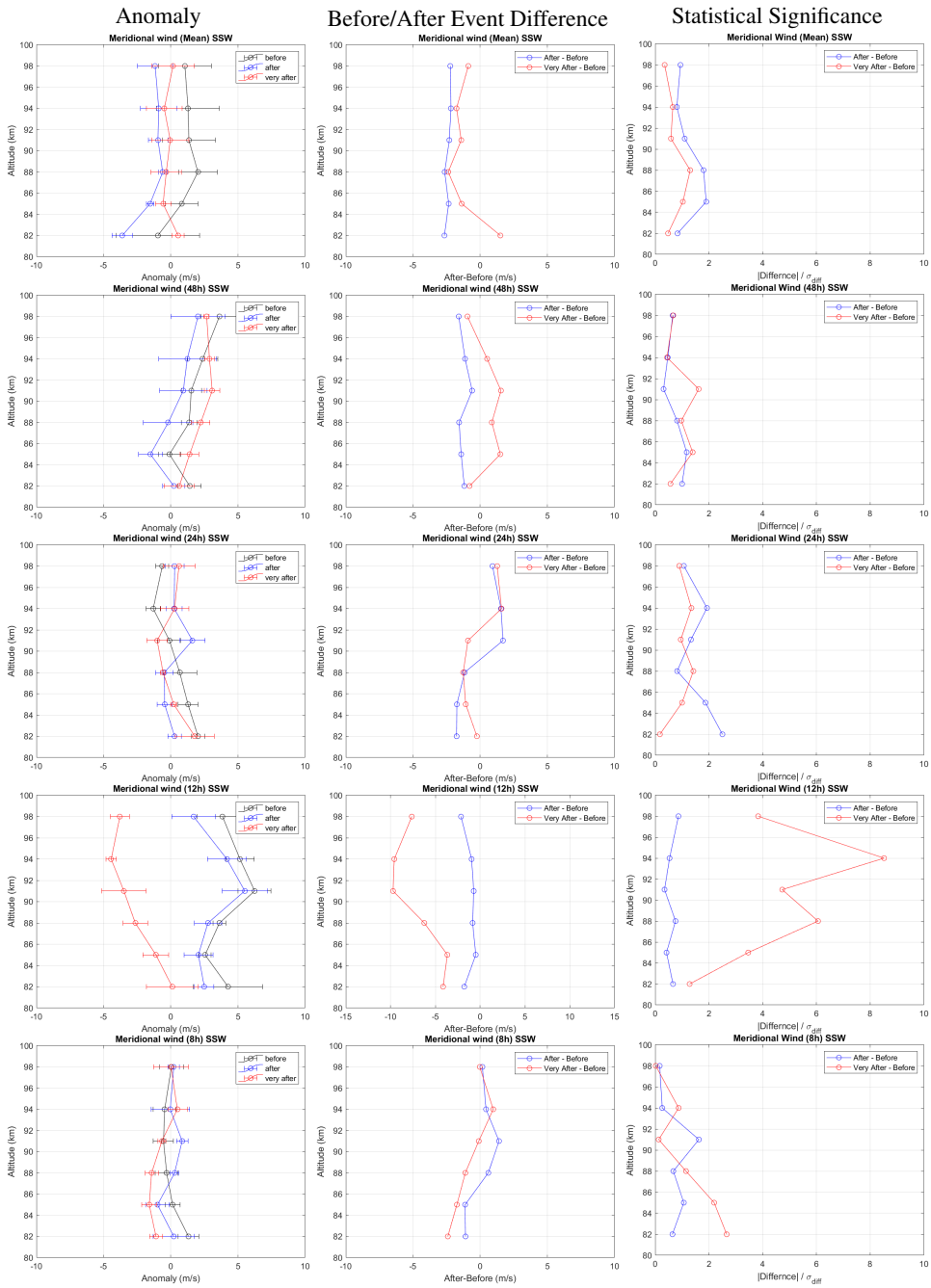

Figure A.7: Statistical analysis using Hibbins-method around SSW onset of Rothera station. From the top, Mean, 48h, 24h, 12h, 8h Merdional tide amplitude

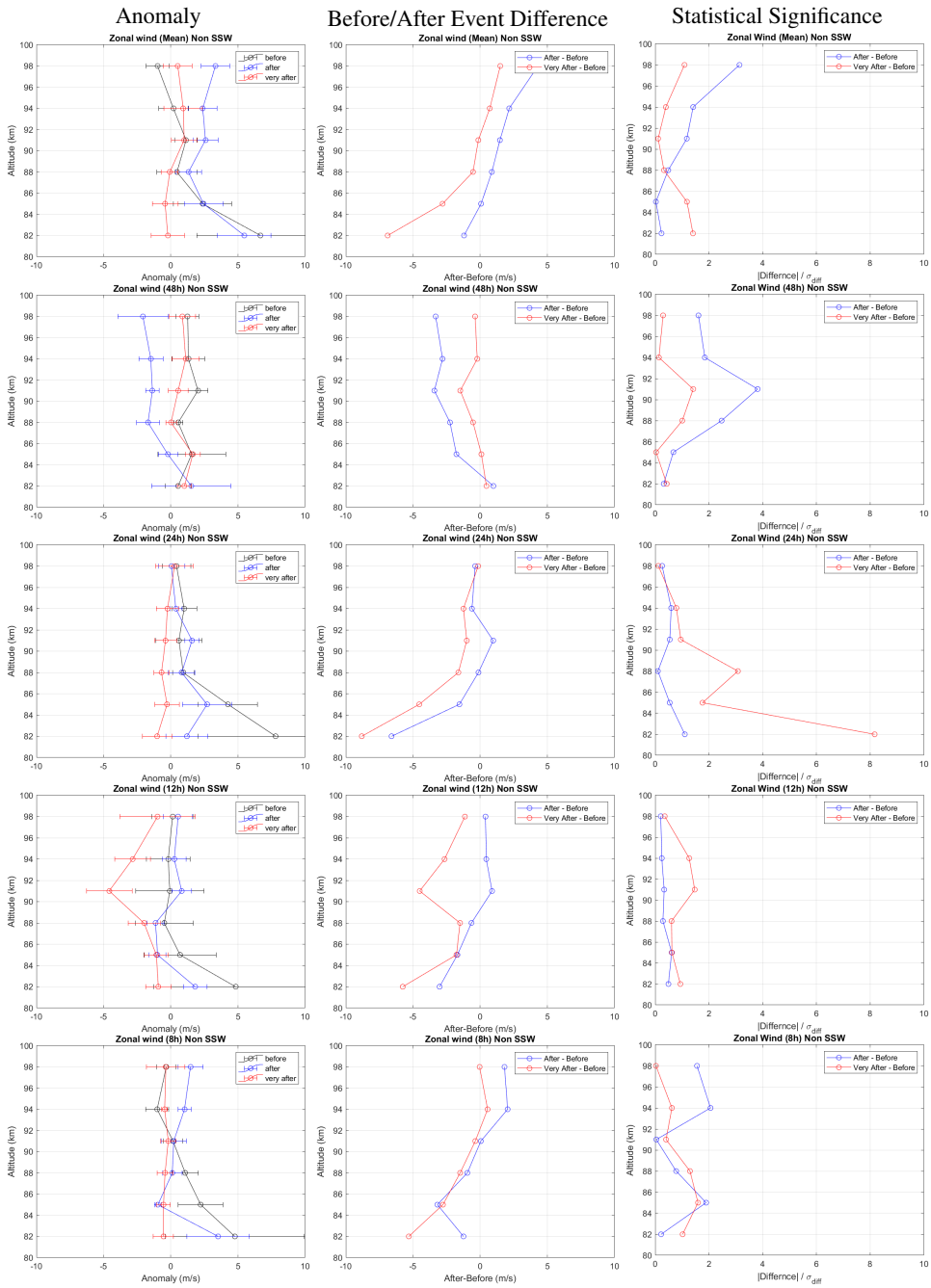

Figure A.8: Statistical analysis using Hibbins-method around random non-SSW onset of Rothera station. From the top, Mean, 48h, 24h, 12h, 8h zonal tide amplitude

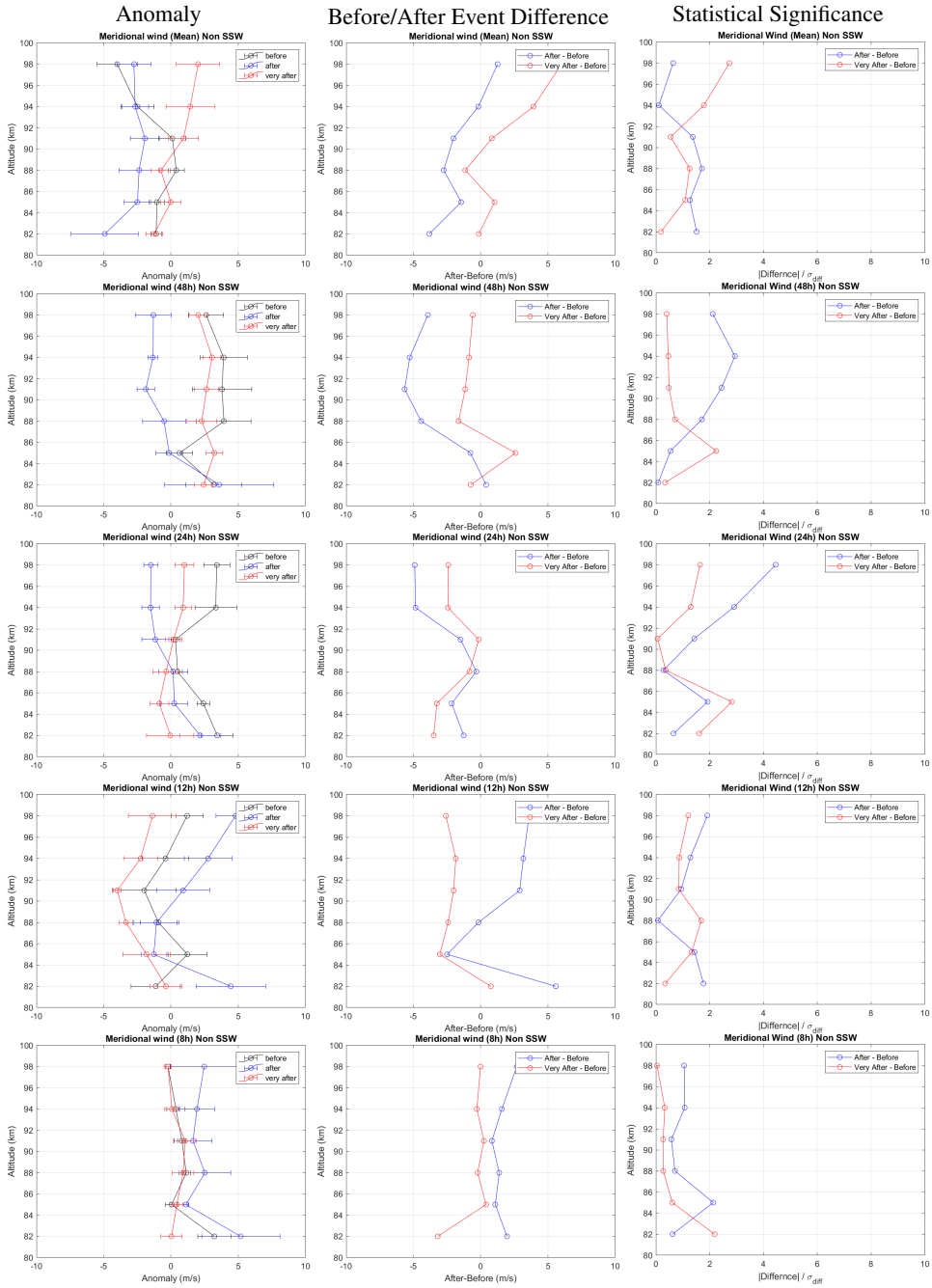

Figure A.9: Statistical analysis using Hibbins-method around random non-SSW onset of Rothera station. From the top, Mean, 48h, 24h, 12h, 8h Meridional tide amplitude

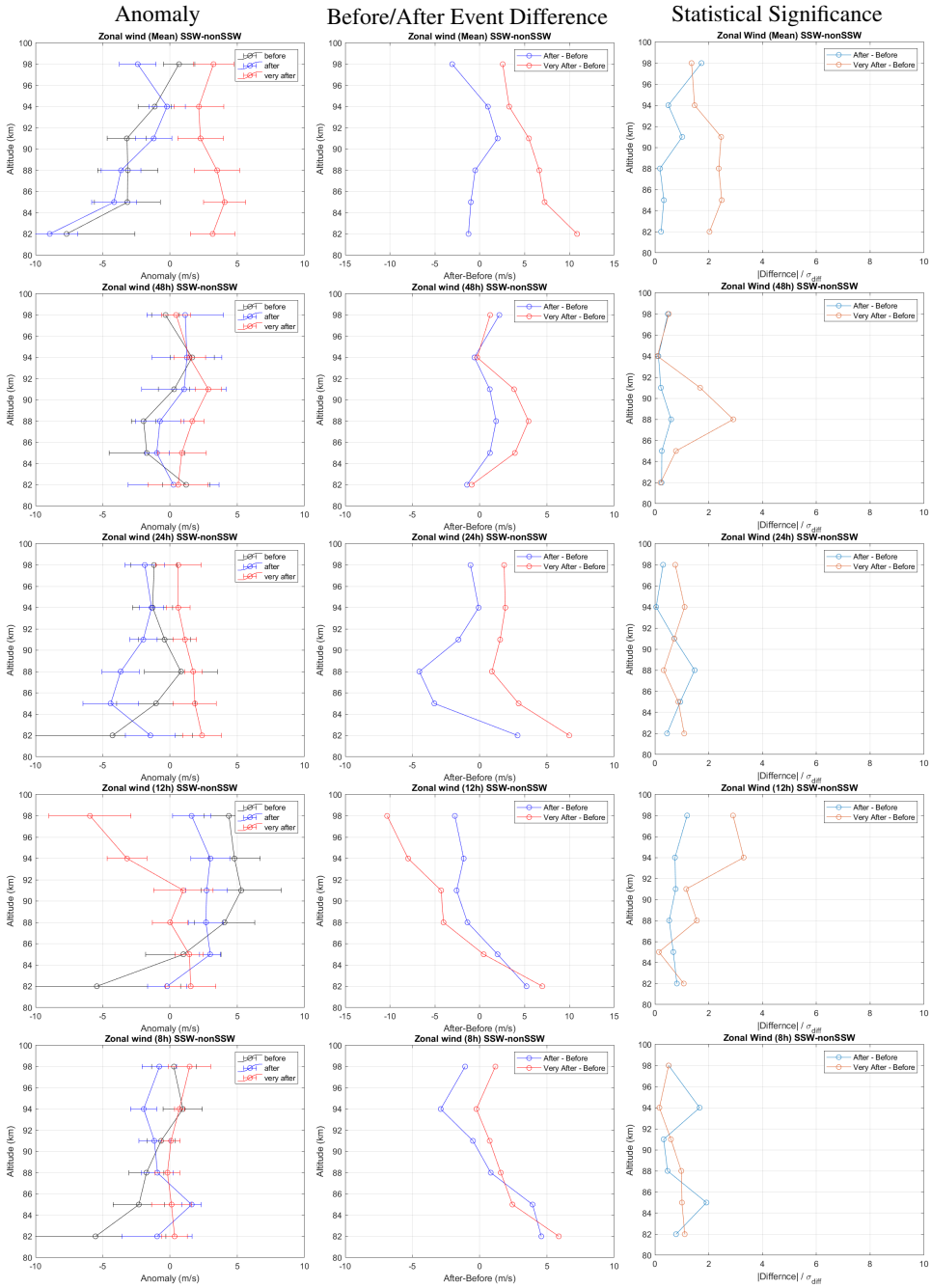

Figure A.10: Subtraction of non-SSW onset from SSW onset for the Statistical analysis of Rothera station. From the top, Mean, 48h, 24h, 12h, 8h Zonal tide amplitude

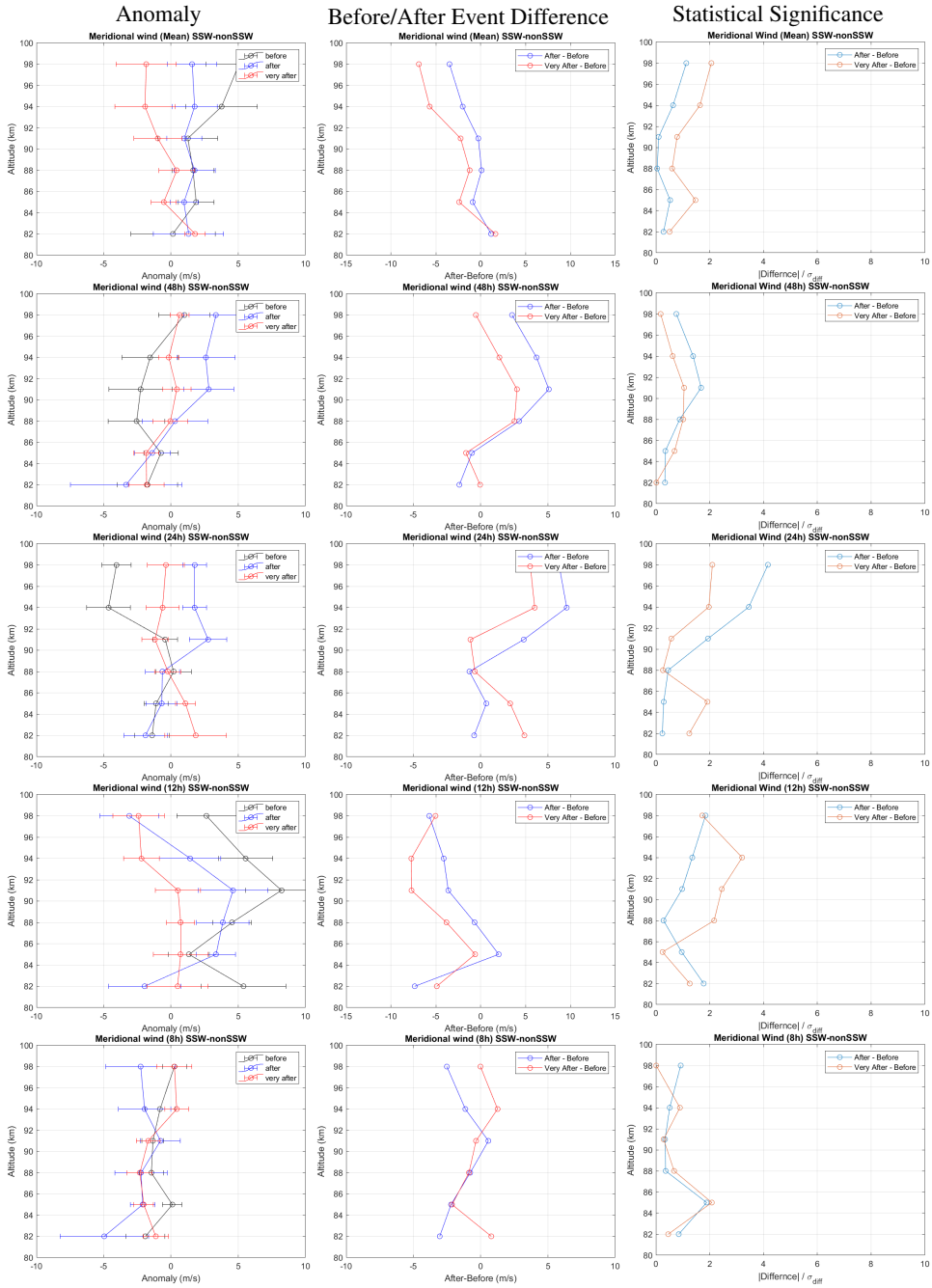

Figure A.11: Subtraction of non-SSW onset from SSW onset for the Statistical analysis of Rothera station. From the top, Mean, 48h, 24h, 12h, 8h Meridional tide amplitude

A.2 Dst Onset

Onset magnitudes and dates used for this project is shown.

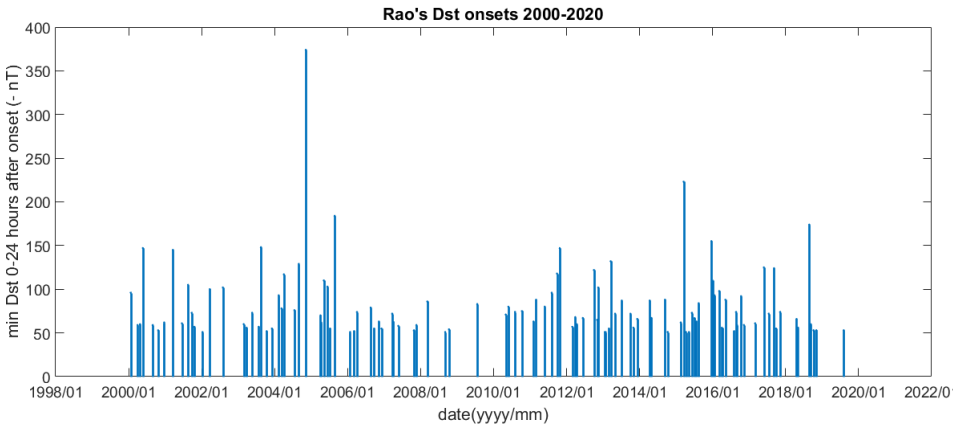

Figure A.12: Onset times and magnitudes for Dst

year	month	day	hour	year	month	day	hour
2005	4	4	14	2013	4	30	20
2005	4	11	18	2013	7	5	19
2005	5	7	21	2013	10	1	20
2005	6	11	21	2013	10	30	1
2005	7	9	7	2013	12	8	2
2005	8	23	22	2014	4	11	13
2006	1	25	18	2014	4	29	22
2006	3	6	18	2014	9	12	0
2006	4	4	11	2014	10	8	9
2006	8	19	1	2015	2	16	22
2006	9	23	8	2015	3	17	6
2006	11	9	20	2015	4	9	23
2006	12	5	14	2015	5	10	6
2007	3	23	10	2015	6	8	5
2007	3	31	13	2015	7	4	18
2007	5	22	17	2015	7	22	22
2007	10	25	14	2015	8	15	10
2007	11	20	10	2015	12	20	4
2008	3	8	12	2015	12	31	11
2008	9	3	10	2016	1	20	5
2008	10	11	2	2016	3	6	16
2009	7	21	5	2016	4	2	16
2010	5	2	11	2016	4	12	9
2010	5	28	21	2016	5	8	1
2010	8	3	2	2016	8	2	21
2010	10	11	9	2016	8	23	12
2011	2	4	3	2016	8	31	18
2011	3	1	10	2016	10	12	14
2011	5	27	11	2016	11	10	1
2011	8	4	23	2017	3	1	9
2011	9	26	15	2017	5	27	22
2011	10	24	14	2017	7	16	7
2012	2	27	1	2017	9	7	8
2012	3	27	9	2017	9	27	7
2012	4	12	4	2017	11	7	7
2012	6	11	4	2018	4	20	4
2012	9	30	14	2018	5	5	1
2012	11	1	4	2018	8	25	17
2012	11	13	4	2018	9	10	11
2013	1	16	21	2018	10	7	12
2013	1	25	23	2018	11	4	11
2013	2	28	13	2019	8	5	6
2013	3	17	6				

Table A.1: The list of dates and hours of Dst onsets used for analysis